Modulation of Reactive Oxygen Species Photogeneration of Bacteriopheophorbide a Derivatives by Exocyclic E-Ring Opening and Charge Modifications

ARTICLE *in* JOURNAL OF MEDICINAL CHEMISTRY · DECEMBER 2013

Impact Factor: 5.45 · DOI: 10.1021/jm401538h · Source: PubMed

5 AUTHORS, INCLUDING:

Aron Roxin
University of Toronto
10 PUBLICATIONS **89** CITATIONS
SEE PROFILE

Juan Chen
University Health Network
72 PUBLICATIONS **1,817** CITATIONS
SEE PROFILE

Andrew S. Paton
University of Toronto
25 PUBLICATIONS **201** CITATIONS
SEE PROFILE

Gang Zheng
Zhejiang University
171 PUBLICATIONS **3,191** CITATIONS
SEE PROFILE

Journal of Medicinal Chemistry

Article

pubs.acs.org/jmc

Modulation of Reactive Oxygen Species Photogeneration of Bacteriopheophorbide *a* Derivatives by Exocyclic E-Ring Opening and Charge Modifications

Áron Roxin,[†,‡] Juan Chen,[‡] Andrew S. Paton,[§] Timothy P. Bender,[§] and Gang Zheng*[,†,‡]

[†]Department of Pharmaceutical Sciences, Leslie L. Dan Faculty of Pharmacy, University of Toronto, 144 College Street, Toronto, Ontario M5S 3M2, Canada

[‡]Ontario Cancer Institute and Techna Institute, UHN, 101 College Street, Toronto, Ontario M5G 1L7, Canada

[§]Department of Chemical Engineering and Applied Chemistry, University of Toronto, 200 College Street, Toronto, Ontario M5S 3E5, Canada

Supporting Information

ABSTRACT: With the knowledge that the dominant photodynamic therapy (PDT) mechanism of **1a** (WST09) switched from type 2 to type 1 for **1b** (WST11) upon taurine-driven E-ring opening, we hypothesized that taurine-driven E-ring opening of bacteriochlorophyll derivatives and net-charge variations would modulate reactive oxygen species (ROS) photogeneration. Eight bacteriochlorophyll *a* derivatives were synthesized with varying charges that either contained the E ring (**2a**–**5a**) or were synthesized by taurine-driven E-ring opening (**2b**–**5b**). Time-dependent density functional theory (TDDFT) modeling showed that all derivatives would be type 2 PDT-active, and ROS-activated fluorescent probes were used to investigate the photogeneration of a combination of type 1 and type 2 PDT ROS in organic- and aqueous-based solutions. These investigations validated our predictive modeling calculations and showed that taurine-driven E-ring opening and increasing negative charge generally enhanced ROS photogeneration in aqueous solutions. We propose that these structure–activity relationships may provide simple strategies for designing bacteriochlorins that efficiently generate ROS upon photoirradiation.

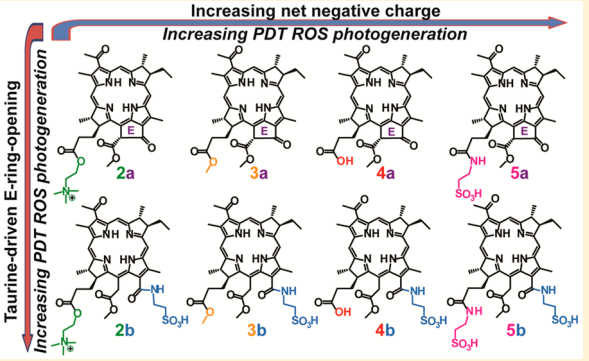

INTRODUCTION

Photosensitizers (PSs) are compounds that generate reactive oxygen species (ROS) upon photoirradiation. PSs have been used for anticancer and antimicrobial applications because of their ability to damage nearby cells by ROS generated through the process of photodynamic therapy (PDT).[1−5] Among their qualifications, ideal PSs should be inactive until the time of irradiation, should be soluble in aqueous solutions, and should efficiently generate ROS.[6] In addition, the wavelength of excitation should be within the PDT optical window (650–850 nm) to maximize the depth of tissue penetration and to minimize the absorption of excitation light by water and hemoglobin in vivo.[1−3,7] PSs can generate ROS by excited-state energy transfer to molecular O_2 (type 2 PDT) to produce singlet oxygen ($^1O_2$) or by excited-state electron transfer to oxygen substrates (type 1 PDT) to generate radicals, peroxides, and superoxide radical anions.[7] Typical PSs undergo type 2 PDT;[5] however, PSs that exclusively undergo type 2 PDT will become inactive when O_2 is depleted from the local irradiated region.[8,9] To circumvent this dependence on O_2, the type 1 PDT mechanism can be explored. This presents a challenge because strategies to design novel PSs with enhanced type 1 and type 2 PDT mechanisms are elusive.[10]

Bacteriochlorins are a class of tetrapyrrole macrocycles with two unsaturated pyrrolic rings that typically have a Q_y absorption band within the PDT optical window at ∼750 nm in the near-infrared (NIR) range. This property allows in vivo tissue penetration to ∼8 mm,[11] which makes bacteriochlorins a useful class of PSs for PDT. Two clinically evaluated bacteriochlorins include **1a** (WST09) and **1b** (WST11) (Chart 1). Compound **1a** is synthesized from palladium insertion into the precursor, bacteriopheophorbide *a* (**4a**).[12] Compound **1a** is a highly potent PS,[13−16] with a triplet excited-state quantum yield (Φ_T) of ∼0.99 that primarily undergoes type 2 PDT in organic solutions.[17] It is the precursor of **1b** that is synthesized by taurine-driven exocyclic E-ring opening at the 13[1]-carbon position of **1a**.[18,19] Compound **1b** is also a highly potent PS,[19−23] and recent investigations found that **1b** primarily undergoes type 1 PDT in aqueous solutions.[24]

Received: October 29, 2013

   dx.doi.org/10.1021/jm401538h | J. Med. Chem. XXXX, XXX, XXX–XXX

Chart 1. Dominant PDT Mechanisms of 1a and 1b

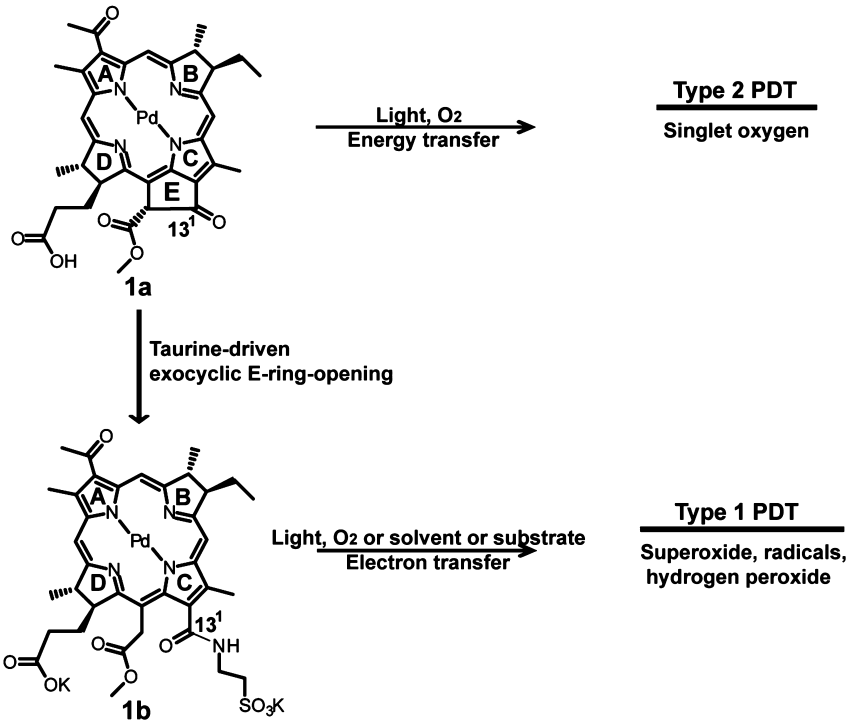

Chart 2. Structures of Bacteriochlorins Synthesized in This Study

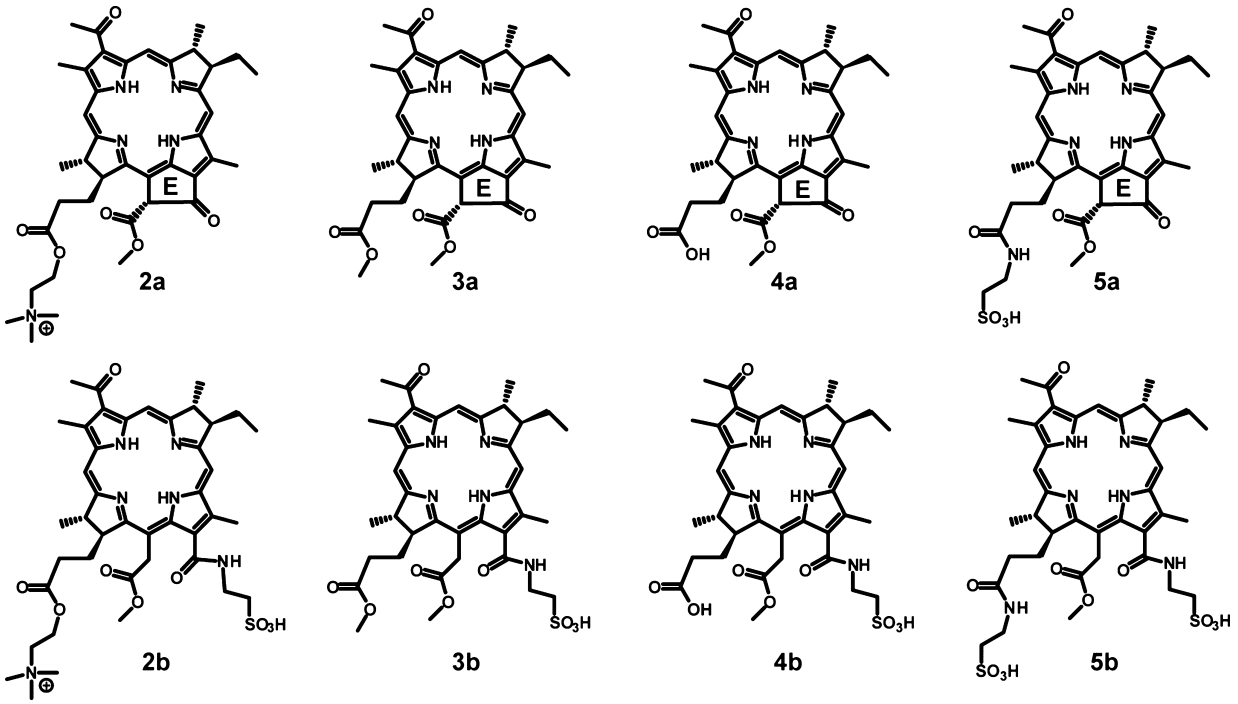

It is currently unclear why the dominant PDT mechanism of **1a** (type 2) switches to type 1 PDT upon taurine-driven exocyclic E-ring opening (**1b**). However, this observation suggests that (i) exocyclic E-ring opening and/or (ii) variations in net charge may influence the PDT mechanisms of bacteriochlorins. To this end, we designed and synthesized a series of eight bacteriochlorophyll *a* derivatives (Chart 2) to investigate the influence of these two potential PDT-modulating factors on the photogeneration of ROS. These bacteriochlorins were chosen to investigate (i) the effect of taurine-driven exocyclic E-ring opening by pairing compounds with and without the exocyclic E ring between the 13- and 15-carbon positions (**2a** vs **2b**, **3a** vs **3b**, **4a** vs **4b**, and **5a** vs **5b**) and (ii) the effect of net charge by conjugating charged moieties at the 17^3-carbon position of compounds with (**2a**–**5a**) and without the exocyclic E ring (**2b**–**5b**).

The spectroscopic properties of the bacteriochlorin series were first characterized to elucidate the effect of taurine-driven

dx.doi.org/10.1021/jm401538h | J. Med. Chem. XXXX, XXX, XXX–XXX

Scheme 1. Synthesis of Bacteriochlorins 1a−3a, 5a, and 1b−5b[a]

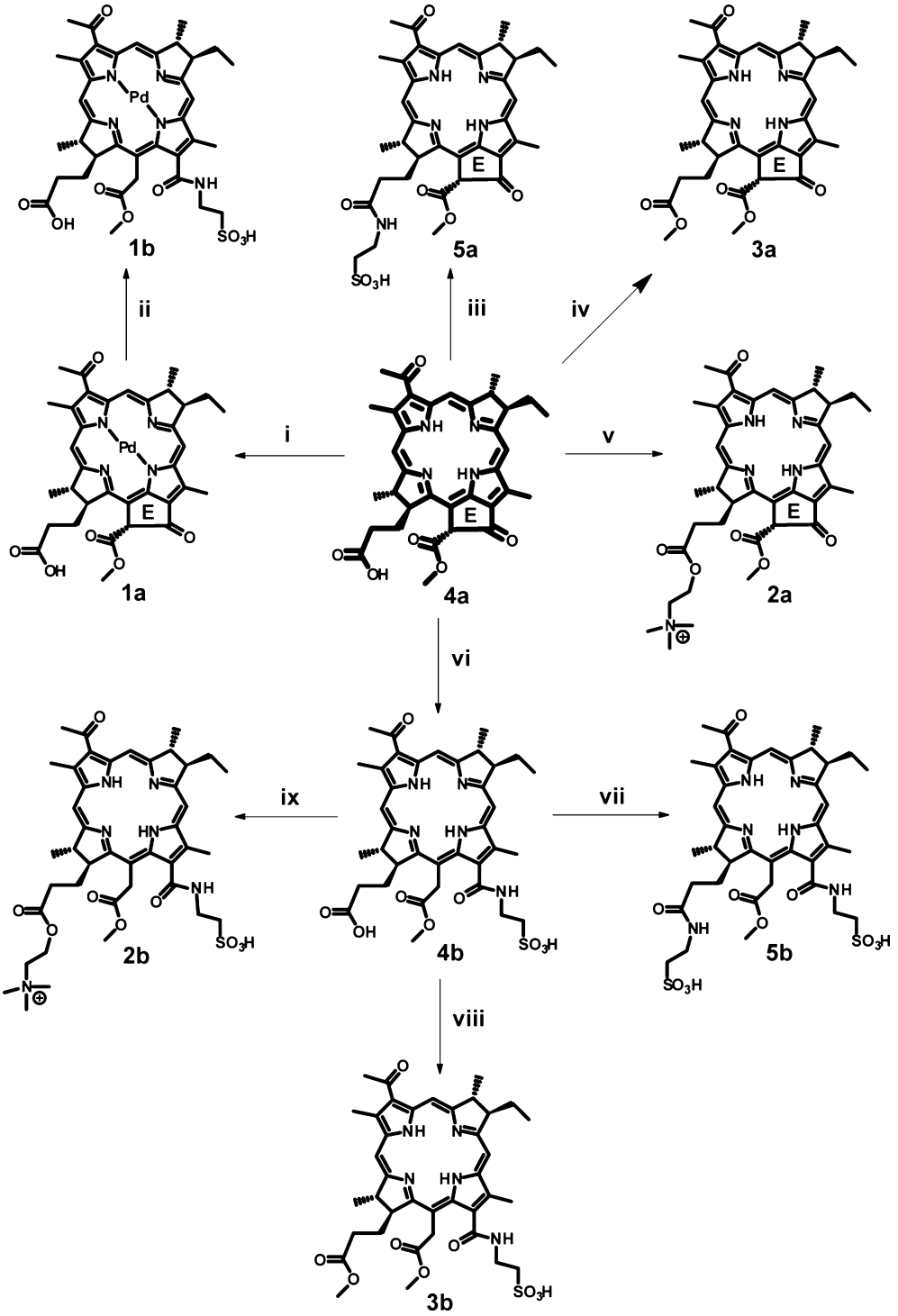

[a]Reaction conditions: (i) $Pd(OAc)_2$, sodium ascorbate, DCM, MeOH, Ar(g). (ii) Taurine, K_2HPO_4(aq) (pH 8.2), DCC, DMAP, DMSO, N_2(g). (iii) Taurine, K_2HPO_4(aq) (pH 8.2), HBTU, DMSO, Ar(g), 40 °C. (iv) MeOH, HBTU, DMAP, DMSO, N_2(g). (v) Choline chloride, HBTU, DMAP, DIPEA, DMSO, Ar(g). (vi) Taurine, K_2HPO_4(aq) (pH 8.2), DCC, DMAP, DMSO, N_2(g). (vii) Taurine, K_2HPO_4(aq) (pH 8.2), HBTU, DMSO, Ar(g), 40 °C. (viii) MeOH, HBTU, DMAP, DMSO, Ar(g). (ix) Choline chloride, HBTU, DMAP, DIPEA, ACN, Ar(g).

exocyclic E-ring opening on the absorbance and fluorescence properties of **2b−5b** compared to **2a−5a**, respectively. Density functional theory (DFT)-based molecular modeling (B3LYP/6-31G*)[25−27] and NMR spectroscopy were then performed to investigate if taurine-driven exocyclic E-ring opening modulated molecular orbital energies and aromatic ring current to alter the absorbance spectra. Although the spectroscopic properties of **2a−5a** and **2b−5b** were explored, the primary goal of this study was to investigate if taurine-driven exocyclic E-ring opening of bacteriochlorophyll *a* derivatives and net-charge variations would modulate ROS photogeneration. Using the time-dependent extension of DFT (TDDFT),[28−36] the vertical

dx.doi.org/10.1021/jm401538h | J. Med. Chem. XXXX, XXX, XXX−XXX

Table 1. Photophysical Characterizations of the Bacteriochlorins 2a−5a and 2b−5b

compound	Q_y λ_{max} (nm)[a]	Q_x λ_{max} (nm)[a]	λ_{em} (nm)[b]	Φ_f[c]	HOMO-to-LUMO gap (eV)[d]	HOMO−1-to-LUMO gap (eV)[d]
2a	745	527	769	0.04	2.05	2.47
2b	749	517	760	0.03	2.10	2.58
3a	748	527	765	0.02	2.05	2.47
3b	749	517	757	0.01	2.13	2.62
4a	744	527	773	0.03	2.05	2.47
4b	749	518	771	0.04	2.08	2.53
5a	747	528	776	0.03	2.05	2.48
5b	750	518	761	0.02	2.13	2.61

[a]MeOH. [b]MeOH (λ_{ex} = 525 nm). [c]MeOH (λ_{ex} = 525 nm; λ_{em} = 700−900 nm), using **1a** as a standard (Φ_f = 0.004).[40] [d]B3LYP/6-31G* (SPARTAN 06).

excited-state energy was calculated to determine whether **2a**−**5a** and **2b**−**5b** showed the potential for type 2 PDT ROS photogeneration.[33−35] ROS-activated fluorescence probes were then used to elucidate experimentally the relative photogeneration of ROS in organic-based solution, aqueous-based solution, and cell culture media. These experimental results were then analyzed to delineate the effects of taurine-driven exocyclic E-ring opening and net-charge variations on ROS photogeneration. The summary of our observations were then used to express structure−activity relationships and to propose simple structural modifications for enhancing the ROS photogeneration of free-base bacteriochlorins.

RESULTS

Synthesis of Bacteriochlorins. The PS, bacteriopheophorbide *a* (**4a**), was synthesized according to literature procedures.[37,38] Briefly, bacteriochlorophyll *a* was extracted from a bacterial culture of *Rhodobacter sphaeroides*, demetalated with dilute HCl(aq), and subsequently hydrolyzed with concentrated TFA(aq) to cleave the phytyl group at the 17^3-carbon position to produce **4a**. These methods gave 942 mg (1.54 mmol) of **4a**, which was used as the precursor for all of the bacteriochlorins in this study (Scheme 1). The net charge of the exocyclic E-ring-containing bacteriochlorins was adjusted by conjugating charge-modifying moieties at the 17^3-carbon position of **4a**. The cationic choline moiety was conjugated to **4a** on the 70 mg scale by esterification according to literature procedures[39] to synthesize 3^1-oxo-rhodobacteriochlorin 17^3-(2-trimethylaminoethyl)ester (**2a**) with a 14% yield (Scheme 1, step v). The carboxylic acid moiety of **4a** was esterified on the 40 mg scale with MeOH to synthesize the neutral 3^1-oxo-rhodobacteriochlorin 17^3-methyl ester (**3a**) with a 34% yield (Scheme 1, step iv). The anionic taurine moiety was conjugated to **4a** on the 25 mg scale by amide conjugation under mildly basic conditions to synthesize 3^1-oxo-rhodobacteriochlorin 17^3-(2-sulfethyl)amide (**5a**) with a 54% yield (Scheme 1, step iii). These reactions generated bacteriochlorins **2a**, **3a**, **4a**, and **5a**, which contained the exocyclic E ring and varied depending on the charged moiety at the 17^3-carbon position. Using a combination of 1D ^{1}H NMR, 2D COSY ^{1}H NMR, ^{13}C Jmod NMR, and HPLC−MS, the identities and purities of the exocyclic E-ring-containing free-base bacteriochlorins **2a**−**5a** were elucidated (Figure S1−S16).

Taurine-driven exocyclic E-ring opening at the 13^1-carbon position of **4a** was achieved according to literature procedures[18,19] with the addition of DCC and DMAP. Taurine was conjugated to **4a** under mildly basic conditions on the 80 mg scale to synthesize 3^1-oxo-15-methoxycarbonylmethyl-rhodobacteriochlorin 13′-(2-sulfethyl)amide (**4b**) with a 37% yield (Scheme 1, step vi). Compound **4b** was then used as the precursor for the synthesis of all other free-base bacteriochlorins that lacked the exocyclic E ring because of taurine conjugation at the 13^1-carbon position. The cationic choline moiety was conjugated to **4b** on the 40 mg scale by esterification at the 17^3-carbon position to synthesize 3^1-oxo-15-methoxycarbonylmethyl-rhodobacteriochlorin 13^1-(2-sulfethyl)amide-17^3-(2-trimethylaminoethyl)ester (**2b**) with a 46% yield (Scheme 1, step ix). The 17^3-carbon position of **4b** was esterified on the 20 mg scale with MeOH to synthesize 3^1-oxo-15-methoxycarbonylmethyl-rhodobacteriochlorin 13′-(2-sulfethyl)amide-17^3-methyl ester (**3b**) with a 59% yield (Scheme 1, step viii). The anionic taurine moiety was conjugated to **4b** on the 39 mg scale by amide conjugation at the 17^3-carbon position under mildly basic conditions to synthesize 3^1-oxo-15-methoxycarbonylmethyl-rhodobacteriochlorin 13^1,17^3-di(2-sulfethyl)amide (**5b**) with a 28% yield (Scheme 1, step vii). These reactions generated bacteriochlorins **2b**, **3b**, **4b**, and **5b** that contained a taurine moiety at the 13^1-carbon position because of exocyclic E-ring opening and varied depending on the charged moiety at the 17^3-carbon position. A combination of 1D ^{1}H NMR, 2D COSY ^{1}H NMR, ^{13}C Jmod NMR, and HPLC−MS was used to elucidate the identities and purities of the free-base bacteriochlorins **2b**−**5b** that were synthesized by taurine-driven exocyclic E-ring opening (Figures S17−S32).

Compound **4a** was used as a precursor for the synthesis of **1a** and **1b**. These two palladium-containing bacteriochlorins were used as controls when assaying the photogeneration of ROS. Compound **1a** was synthesized by palladium insertion into **4a** on the 70 mg scale according to literature procedures[12] with a 69% yield (Scheme 1, step i). Compound **1b** was synthesized by taurine-driven exocyclic E-ring opening at the 13^1-carbon position of **1a** according to literature procedures[18,19] with the addition of DCC and DMAP (Scheme 1, step ii). This reaction generated the product, **1b**, as well as the chlorin analogue of **1b** because of the oxidation of an unsaturated pyrrolic ring. This required purification by HPLC and, consequently, gave a very low (∼ 1%) yield. A combination of 1D ^{1}H NMR, 2D COSY ^{1}H NMR, ^{13}C Jmod NMR, and HPLC−MS (Figure S33) was used to elucidate the identity and purity of **1a**, whereas HPLC−MS was used to characterize **1b** (Figure S34).

Spectroscopic Properties of Bacteriochlorins. The UV−vis absorption spectra of **2a**−**5a** and **2b**−**5b** were recorded in MeOH (Table 1) to investigate if the Q_x bands (500−550 nm) and Q_y bands (725−800 nm) of **2a**−**5a** shifted upon taurine-driven exocyclic E-ring opening (**2b**−**5b**). The results showed that the Q_y bands of **2b**−**5b** are slightly red-shifted (λ_{max} = 749, 750 nm) compared to **2a**−**5a** (λ_{max} = 744, 748

dx.doi.org/10.1021/jm401538h | J. Med. Chem. XXXX, XXX, XXX−XXX

nm), whereas the Q_x bands of **2b**−**5b** are consistently blue-shifted (λ_{max} = 517−518 nm) by 9 to 10 nm compared to **2a**−**5a** (λ_{max} = 527, 528 nm). Molecular modeling at the DFT level was subsequently performed (Tables S1 and S2) using the B3LYP functional and the 6-31G* basis set, as implemented in SPARTAN 06, to calculate the HOMO-to-LUMO and the HOMO−1-to-LUMO energy gaps of **2a**−**5a** and **2b**−**5b**[25,26] to explain the minor Q_y band shifts and the consistent Q_x band shifts, respectively,[27] observed upon taurine-driven exocyclic E-ring opening (Table 1). The calculated HOMO-to-LUMO energy gaps of the derivatives containing the exocyclic E ring (**2a**−**5a**) were slightly greater (0.02387−0.08016 eV) than that of their respective derivatives without the exocyclic E ring (**2b**−**5b**), which could not explain the bathochromic Q_y band shifts. However, the low magnitude of the HOMO-to-LUMO energy gaps (less than 0.1 eV) was consistent with the minor Q_y band shifts (less than 5 nm). Conversely, taurine-driven exocyclic E-ring opening consistently increased the energy gaps of HOMO−1 to LUMO between **2a** and **2b** (0.11 eV), **3a** and **3b** (0.15 eV), **4a** and **4b** (0.06 eV), and **5a** and **5b** (0.14 eV), which resulted in the consistent hypsochromic shifts of the Q_x bands of **2b**−**5b** compared to **2a**−**5a**.

The local electron densities at the C ring, adjacent to the exocyclic E ring of **2a**−**5a** and adjacent to the conjugated taurine moiety at the 13^1-carbon position of **2b**−**5b**, were further investigated by ^{1}H NMR analysis to determine if taurine-driven exocyclic E-ring opening modulated aromatic-ring currents to increase the HOMO−1-to-LUMO gap energies of **2b**−**5b** compared to **2a**−**5a**. It was found that the H23-NH protons (δ = +0.70 to +0.47 ppm) were consistently deshielded compared to the H21-NH protons (δ = −0.82 to −0.96 ppm) in **2a**−**5a** that contained the coplanar electron-withdrawing ketone substituent[41] within the exocyclic E ring (Table 2).

Table 2. ^{1}H NMR Shifts (δ = ppm, DMSO-d_6) of H21-NH and H23-NH of 2a−5a and 2b−5b

compound	exocyclic E-ring status	H21-NH	H23-NH
2a	present	−0.82	+0.70
2b	not-present	−1.32	−1.32
3a[a]	present	−0.95	+0.48
3b	not-present	−1.32	−1.31
4a	present	−0.96	+0.47
4b	not-present	−1.30	−1.30
5a	present	−0.84	+0.68
5b	not-present	−1.29	−1.28

[a]$CDCl_3$

Upon taurine-driven exocyclic E-ring opening, the H21-NH and H23-NH protons became shifted upfield (δ = −1.28 to −1.32 ppm) in the spectra of **2b**−**5b** because of the relatively increased shielding at the adjacent C ring. This showed that the amide substituent at the 13^1-carbon position in **2b**−**5b** displayed a lower electron-withdrawing effect on the H23-NH protons compared to the coplanar ketone substituent within the exocyclic E ring of **2a**−**5a**. These results suggest that the local electron density at the C ring increased between compounds **2a** and **2b**, **3a** and **3b**, **4a** and **4b**, and **5a** and **5b**. Therefore, these local electron-density enhancements modulated aromatic-ring currents and contributed to the increased HOMO−1-to-LUMO energy gaps and the hypsochromic Q_x band shifts of **2b**−**5b** compared to **2a**−**5a** (Figure 1).

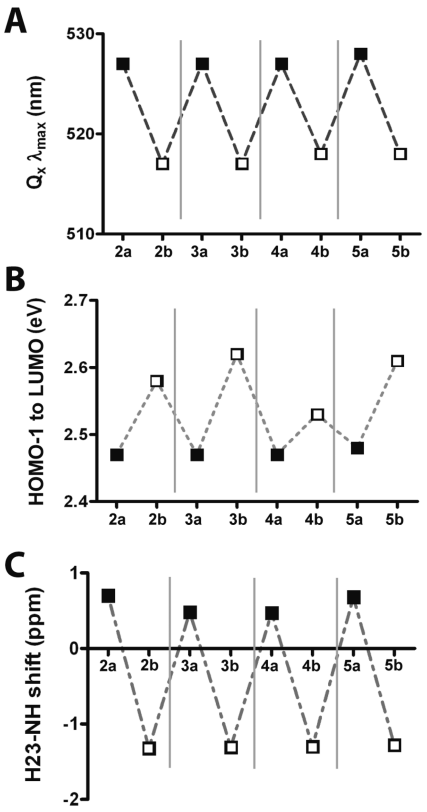

Figure 1. Correlation of (A) Q_x λ_{max} (MeOH), (B) B3LYP/6-31G* (SPARTAN 06) calculated HOMO−1-to-LUMO energy gap, and (C) ^{1}H NMR shift of H23-NH as a result of the presence (■; **2a**−**5a**) or absence (□; **2b**−**5b**) of the exocyclic E ring.

The fluorescence properties of **2a**−**5a** and **2b**−**5b** were investigated in MeOH to elucidate the effect of taurine-driven exocyclic E-ring opening on the fluorescence spectra and the fluorescence quantum yields (Φ_f) (Table 1). Analysis of the fluorescence spectra showed that the maximum emission wavelengths of the bacteriochlorins are consistently blue-shifted upon taurine-driven exocyclic E-ring opening: 9 (**2a** vs **2b**), 8 (**3a** vs **3b**), 2 (**4a** vs **4b**), and 15 nm (**5a** vs **5b**). Consequently, their Stokes shifts are slightly decreased: 13 (**2b** vs **2a**), 9 (**3b** vs **3a**), 7 (**4b** vs **4a**), and 18 nm (**5b** vs **5a**). These fluorescence results suggest that taurine-driven exocyclic E-ring opening had a minor effect on the singlet excited-state rigidity.[42−47] Further investigations of the Φ_f values of **2a**−**5a** (Φ_f = 0.02 − 0.04) and **2b**−**5b** (Φ_f = 0.01 − 0.04) showed that taurine-driven exocyclic E-ring opening had little effect on Φ_f. Therefore, potential variations of ROS photogeneration of **2a**−**5a** compared to **2b**−**5b** would not be primarily because of modulations of the quantum yields of internal conversion (Φ_{IC})[42−47] or Φ_f.

Molecular Modeling of Potential PDT Activity. Time-dependent DFT (TDDFT) methods were employed to calculate the vertical excitation energies of **2a**−**5a** and **2b**−**5b** to estimate whether the compounds were photodynamically active. According to literature procedures, the use of TDDFT with the B3LYP functional and the 6-31G* basis set provides a useful estimate of the energy difference between the singlet ground-state (S_0) and the vertical triplet excited state.[30,31,34] We optimized the geometry using symmetry-unrestricted DFT methods at B3LYP/6-31G* and then performed single-point energy calculations using TDDFT methods at the same level of

dx.doi.org/10.1021/jm401538h | J. Med. Chem. XXXX, XXX, XXX−XXX

theory to determine the vertical excitation energies of **2a−5a** and **2b−5b**.[32−36] The calculations were performed in the gas phase because it has been shown that for excitation calculations at this level the effects of the solvent are negligible.[28,29] These calculations were used to investigate the potential of these bacteriochlorins to generate type 2 PDT ROS. Type 2 PDT require the vertical singlet−triplet excitation energy gap (ΔE^{ST}) of PSs to be greater than 0.98 eV to transfer energy from their triplet excited state to ground-state molecular oxygen ($^3O_2$) to produce singlet oxygen ($^1O_2$).[33−35] These ΔE^{ST} calculations showed that **2a−5a** and **2b−5b** were each capable of undergoing type 2 PDT (Table S3) and that the ΔE^{ST} values of the compounds without the exocyclic E ring (**2b−5b**: ΔE^{ST} = 1.5445−1.6218 eV) are consistently higher than that of compounds with the exocyclic E ring (**2a−5a**; ΔE^{ST} = 1.4926−1.5172 eV) (Figure 2).

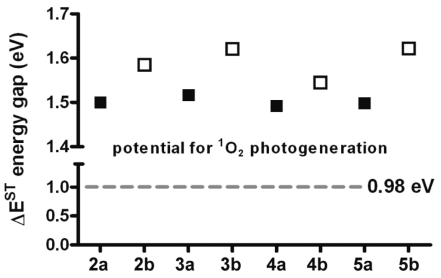

Figure 2. Calculated ΔE^{ST} energy gap (B3LYP/6-31G*) for compounds with (■; **2a−5a**) and without (□; **2b−5b**) the exocyclic E ring.

ROS Photogeneration Detected with AUR. We next experimentally investigated the relative ROS photogeneration of **2a−5a** and **2b−5b** using the ROS-activated fluorescent probe Amplex UltraRed (AUR).[48−52] Compounds **1a** and **1b** were used as controls. It was found that the known hydrogen peroxide quencher dimethyl thiourea (DMTU),[53−55] the known superoxide quencher 1,2-dihydroxybenzene-3,5-disulfonic acid disodium salt hydrate (tiron),[56−58] and the known singlet oxygen quencher sodium azide[59,60] could quench the fluorescence of AUR while irradiating compound **4a** with a 740 nm LED light box in 70:17.5:12.5 H_2O/cremophor/DMF (v/v) (Figure S35A), indicating that AUR could detect both type 1 (superoxide and hydrogen peroxide) and type 2 ($^1O_2$) PDT ROS.

A report by Vakrat-Haglili et al. showed that the known type 2 PDT PS, **1a**, generates significant amounts of type 1 PDT ROS in aqueous solutions but not in organic solutions.[17] This suggests that **1a** would generate different proportions of type 1 and type 2 PDT ROS depending on the aqueous content of the tested solutions. Therefore, our PDT ROS experiments were conducted in a MeOH-based solution, in H_2O with high concentrations of detergents, and in cell culture media appropriate for many cancer cell lines. These solvents were primarily chosen to investigate the ROS photogeneration of **2a−5a** and **2b−5b** in a variety of solvents that differed in aqueous content. These investigations included the use of cell culture media to mimic ROS photogeneration under biocompatible in vitro solution conditions.

AUR was used to investigate ROS photogeneration in 70:30 MeOH/PBS (v/v), 70:17.5:12.5 H_2O/cremophor/DMF (v/v), and 97.5:2:0.5 RPMI-1640 cell culture media/DMSO/cremophor (v/v). The optical density (OD) of the bacteriochlorins was matched with OD_{740} = 0.2, and the compounds were irradiated with a 740 nm LED light box to determine the relative photogeneration of ROS. The photobleaching of PSs was monitored (λ_{Abs} = 740 nm) after each light treatment (ΔAbs_{PS})[61−64] while concomitantly monitoring increasing AUR fluorescence (ΔFlr_{AUR}) to express the relative ROS photogeneration of each PS as the linear slopes (r^2 = 0.859 − 0.9999) of the corrected AUR fluorescence ($\Delta Flr_{AUR}/\Delta Abs_{PS}$) over the light dose range according to literature methods.[64−67] Solutions required either high concentrations of MeOH or detergents to dissolve the bacteriochlorins in this series fully. The particular concentrations of DMSO (2%, v/v) and cremophor (0.5%, v/v) in cell culture media were chosen because these concentrations did not induce toxicity to A549 nonsmall cell lung cancer cells, as indicated by MTT analysis (Figure S36). Consequently, the hydrophobic bacteriochlorins, **3a** and **4a**, were restricted from the cell culture media studies because of aggregation observed by spectral red-shifting of the Q_y absorption bands beyond 800 nm (Figure S37).

Our AUR-based analysis involved pairing derivatives that varied on the basis of exocyclic E-ring status (**2a** vs **2b**, **3a** vs **3b**, **4a** vs **4b**, and **5a** vs **5b**). The results showed that exocyclic E-ring opening enhanced the photogeneration of ROS for **2b** compared to **2a** under all of the tested solution conditions. Specifically, there was a 102% increase ($p < 0.005$) in the MeOH-based solution (Figure 3A), a 47% increase ($p < 0.005$) in H_2O with high detergent concentrations (Figure 3B), and a 52% increase ($p < 0.005$) in cell culture media (Figure 3C) for **2b** compared to **2a**. The photogeneration of ROS was also enhanced for **4b** compared to **4a** in the two tested solutions, including a 33% increase ($p < 0.05$) in the MeOH-based solution (Figure 3A) and a 42% increase ($p < 0.005$) in H_2O with high detergent concentrations (Figure 3B). The photogeneration of ROS also increased for **3b** compared to **3a** by 39% ($p < 0.005$) in the MeOH-based solution (Figure 3A) and for **5b** compared to **5a** by 18% ($p < 0.01$) in H_2O with high detergent concentrations (Figure 3B). In summary, there was a general trend observed wherein taurine-driven exocyclic E-ring opening enhanced the photogeneration of ROS, especially for compounds **2b** (compared to **2a**) and **4b** (compared to **4a**) in solutions containing significant proportions of organic solvent or detergents. A trend was also observed for the palladium-containing compounds, **1a** and **1b**. Specifically, the photogeneration of ROS increased for **1b** compared to **1a** by 36% ($p < 0.001$) in H_2O with high detergent concentrations (Figure 3B) and by 64% ($p < 0.001$) in cell culture media (Figure 3C), whereas no difference was observed in the MeOH-based solution (Figure 3A).

The aforementioned AUR fluorescence results were analyzed to delineate the influence of exocyclic E-ring status and net charge on the photogeneration of ROS in the three aforementioned solutions. Analysis showed that taurine-driven exocyclic E-ring opening significantly enhanced the photogeneration of ROS (**2b−5b** > **2a−5a**) in the MeOH-based solution by 40% ($p < 0.005$), in H_2O with high detergent concentrations by 25% ($p < 0.005$), and in cell culture media by 29% ($p < 0.005$). In addition, the net charge of these bacteriochlorins influenced ROS photogeneration in all of the tested solutions, whereby increasing the net negative charge significantly enhanced ROS photogeneration in the MeOH-based solution (Figure 4A, $p < 0.01$), in H_2O with high detergent concentrations (Figure 4B, $p < 0.005$), and in cell culture media (Figure 4C, $p < 0.005$). Analysis of the predicted

dx.doi.org/10.1021/jm401538h | J. Med. Chem. XXXX, XXX, XXX−XXX

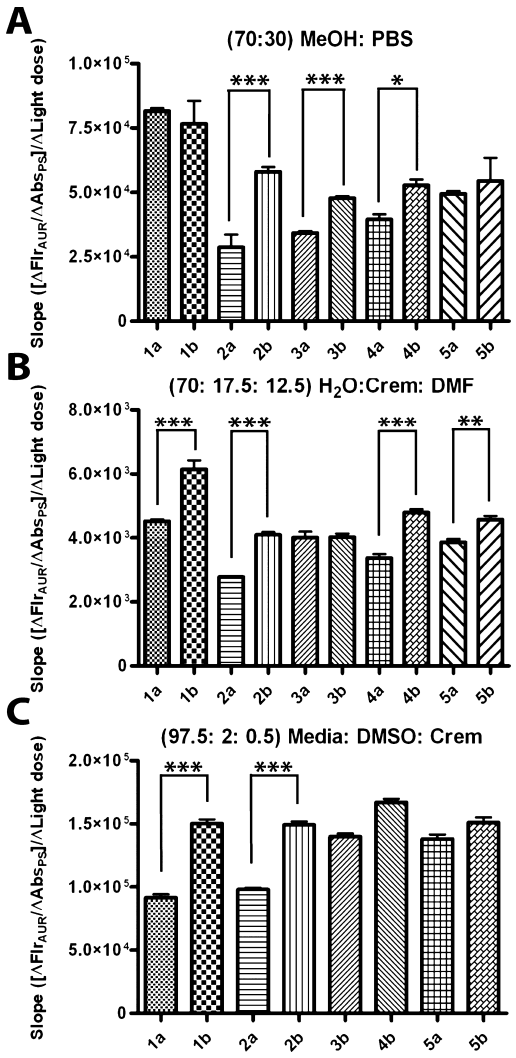

Figure 3. Photogeneration of ROS by bacteriochlorins with (**1a**−**5a**) and without (**1b**−**5b**) the exocyclic E ring indicated by the linear slopes of corrected AUR fluorescence ($\Delta Flr_{AUR}/\Delta Abs_{PS}$) over the light dose range (ΔLight dose) after 740 nm irradiation in MeOH-based solution (A; light dose = 0−100 mJ, $r^2 > 0.986$), in H_2O with high detergent concentrations (B; light dose = 0−1500 mJ, $r^2 > 0.983$), and in cell culture media (C; light dose = 0−100 mJ, $r^2 = 0.859$−0.945) ($n = 3$, error bars show ± SE; * $p < 0.05$, ** $p < 0.01$, and *** $p < 0.005$). Compounds **3a** and **4a** were excluded from assays in cell culture media (C) because of their observed aggregation (Figure S37).

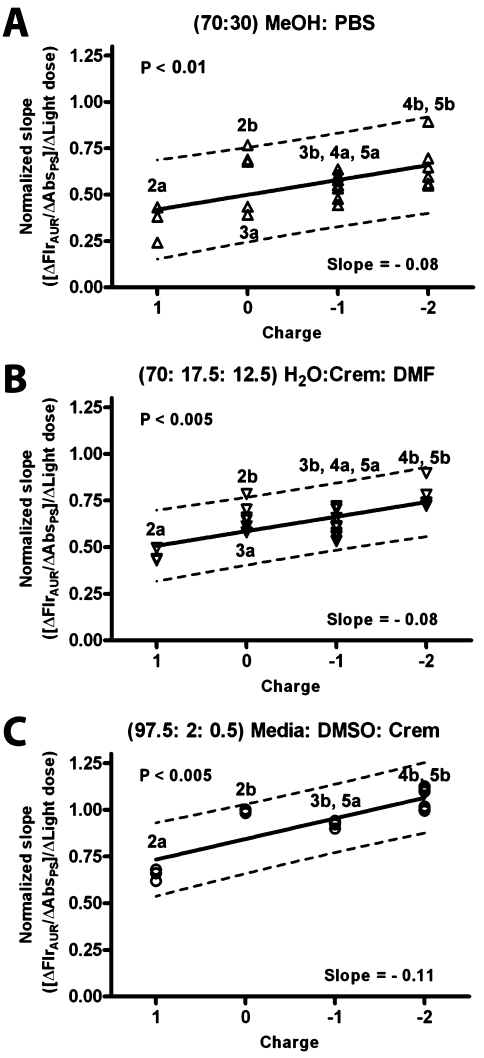

Figure 4. Photogeneration of ROS by bacteriochlorins indicated by the linear slopes of corrected AUR fluorescence ($\Delta Flr_{AUR}/\Delta Abs_{PS}$, normalized to **1b**) over the light dose range (ΔLight dose) after 740 nm irradiation in MeOH-based solution (A; light dose = 0−100 mJ, $r^2 > 0.9841$), in H_2O with high detergent concentrations (B; light dose = 0−1500 mJ, $r^2 > 0.9816$), and in cell culture media (C; light dose = 0−100 mJ, $r^2 = 0.8327$−0.9303) compared to the net charge of derivatives with (**2a**−**5a**) and without (**2b**−**5b**) the exocyclic E ring ($n = 3$, dashed lines show predicted 95% CI). Compounds **3a** and **4a** were excluded from assays in cell culture media (C) because of their observed aggregation (Figure S37).

95% confidence interval (CI) ranges and slopes (fluorescence vs charge) of the regressions showed that the net negative charge was most influential for enhancing ROS photogeneration in cell culture media (Figure 4C, 95% CI range = ±0.2128, slope = −0.11) followed by H_2O with high detergent concentrations (Figure 4B, 95% CI range = ±0.1816, slope = −0.08) and the organic-based solution (Figure 4A, 95% CI range = ±0.2548, slope = −0.08).

ROS Photogeneration Detected with SOSG. The ROS photogeneration of **1a**−**5a** and **1b**−**5b** was investigated using the ROS-activated fluorescent probe Singlet Oxygen Sensor Green (SOSG).[59,64,68−71] Because DMTU, tiron, and sodium azide could quench the fluorescence of SOSG when irradiating compound **4a** with a 740 nm LED light box in 70:17.5:12.5 H_2O/cremophor/DMF (v/v) (Figure S35B), SOSG could be an indicator to determine the presence of both type 1 (superoxide and hydrogen peroxide) and type 2 ($^1O_2$) PDT ROS. This was in agreement with a previous report that showed that SOSG can detect superoxide, hydrogen peroxide, and hydroxyl radicals.[72] SOSG was subsequently used to investigate the ROS photogeneration of the aforementioned bacteriochlorins ($OD_{740} = 0.2$) in 70:30 MeOH/PBS (v/v), 70:17.5:12.5 H_2O/cremophor/DMF (v/v), and 97.5:2:0.5 RPMI-1640 cell culture media/DMSO/cremophor (v/v) after irradiation with a 740 nm LED light box. The photobleaching of PSs was monitored (λ_{Abs} = 740 nm) after each light treatment (ΔAbs_{PS})[61−64] while concomitantly monitoring increasing SOSG fluorescence (ΔFlr_{SOSG}) to express the relative ROS photogeneration of each PS as the linear slopes ($r^2 = 0.92$−0.999) of the corrected SOSG fluorescence

dx.doi.org/10.1021/jm401538h | J. Med. Chem. XXXX, XXX, XXX−XXX

($\Delta Flr_{SOSG}/\Delta Abs_{PS}$) over the light dose range according to literature methods.[64−67]

Our SOSG-based analysis involved pairing derivatives that varied based on exocyclic E-ring status (**2a** vs **2b**, **3a** vs **3b**, **4a** vs **4b**, and **5a** vs **5b**). These investigations showed that taurine-driven exocyclic E-ring opening consistently enhanced the photogeneration of ROS for **2b** compared to **2a** under all of the tested solution conditions. Specifically, there was an 80% increase ($p < 0.01$) in the MeOH-based solution (Figure 5A), a 36% increase ($p < 0.005$) in H_2O with high detergent concentrations (Figure 5B), and a 76% increase ($p < 0.005$) in cell culture media (Figure 5C) for **2b** compared to **2a**. The photogeneration ROS was also consistently enhanced for **5b** compared to **5a** under all of the tested solution conditions. This included a 75% increase ($p < 0.05$) in the MeOH-based solution (Figure 5A), a 28% increase ($p < 0.01$) in H_2O with high detergent concentrations (Figure 5B), and a 26% increase in cell culture media (Figure 5C, $p < 0.005$) for **5b** compared to **5a**. The photogeneration of ROS was also enhanced for **3b** compared to **3a** in the MeOH-based solution by 81% (Figure 5A, $p < 0.05$) and for **4b** compared to **4a** by 43% ($p < 0.005$) in H_2O with high detergent concentrations (Figure 5B). In summary, there was a general trend observed wherein taurine-driven exocyclic E-ring opening enhanced the photogeneration of ROS, especially for compounds **2b** (compared to **2a**) and **5b** (compared to **5a**) in all of the tested solutions. A trend was also observed for the palladium-containing compounds, **1a** and **1b**. Specifically, the photogeneration of ROS increased for **1b** compared to **1a** by 32% ($p < 0.001$) in H_2O with high detergent concentrations (Figure 5B) and by 112% ($p < 0.05$) in cell culture media (Figure 5C), whereas no difference was observed in the MeOH-based solution (Figure 5A).

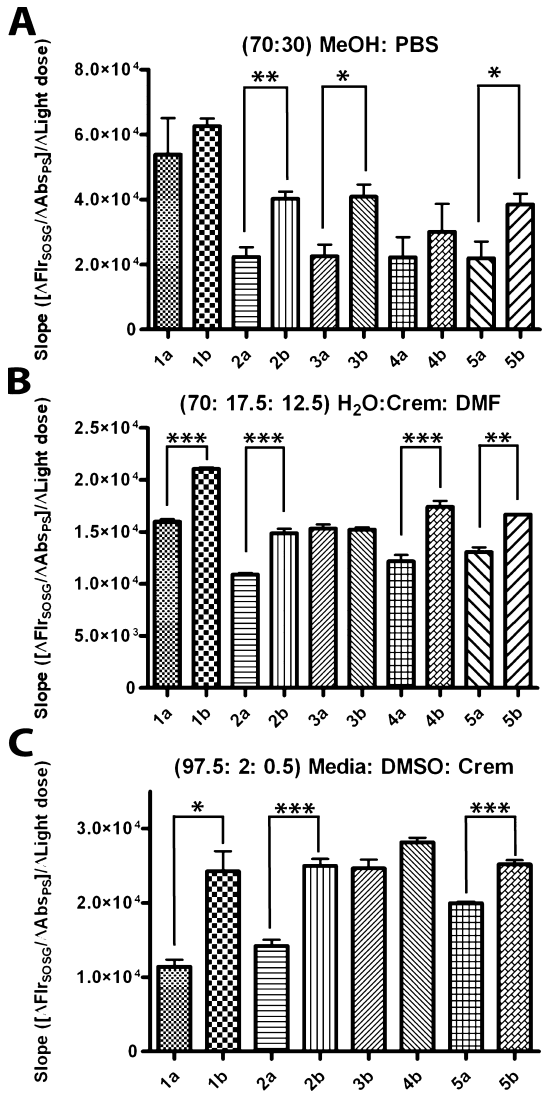

Figure 5. Photogeneration of ROS by bacteriochlorins with (**1a−5a**) and without (**1b−5b**) the exocyclic E ring indicated by the linear slopes of corrected SOSG fluorescence ($\Delta Flr_{SOSG}/\Delta Abs_{PS}$) over the light dose range (ΔLight dose) after 740 nm irradiation in MeOH-based solution (A; light dose = 0−250 mJ, $r^2 = 0.92 - 0.999$), in H_2O with high detergent concentrations (B; light dose = 0−1000 mJ, $r^2 > 0.992$), and in cell culture media (C; light dose = 0−750 mJ, $r^2 > 0.986$) ($n = 3$, error bars show ± SE; * $p < 0.05$, ** $p < 0.01$, and *** $p < 0.005$). Compounds **3a** and **4a** were excluded from assays in cell culture media (C) because of their observed aggregation (Figure S37).

The aforementioned SOSG fluorescence results were analyzed to delineate the influence of exocyclic E-ring status and net charge on the photogeneration of ROS in the three aforementioned solutions. Analysis showed that taurine-driven exocyclic E-ring opening significantly enhanced the photogeneration of ROS (**2b−5b** > **2a−5a**) in the MeOH-based solution by 68% ($p < 0.005$), in H_2O with high detergent concentrations by 25% ($p < 0.005$), and in cell culture media by 51% ($p < 0.005$). However, the net charge of these bacteriochlorins did not consistently influence ROS photogeneration in all of the tested solutions. Analysis of the predicted 95% CI ranges and slopes (fluorescence vs charge) of the regressions showed that increasing net negative charge enhanced ROS photogeneration in H_2O with high detergent concentrations (Figure 6B, $p < 0.005$, 95% CI range = ±0.1736, slope = −0.07) and in cell culture media (Figure 6C, $p < 0.01$, 95% CI range = ±0.5434 slope = −0.15), but was not influential in the organic-based solution (Figure 6A, $p = 0.26$, 95% CI range = ±0.3792, slope = −0.04).

DISCUSSION

The primary objective of our studies was to determine whether taurine-driven exocyclic E-ring opening and net charge would influence the photogeneration of ROS by free-base bacteriopheophorbide *a* derivatives. To this end, eight bacteriochlorins were synthesized that varied in structure because of the presence (**2a−5a**) or absence (**2b−5b**) of the exocyclic E ring and because of net-charge (+1, 0, −1, and −2) variations as a result of moieties conjugated through the 17^3-carbon position and by the taurine moiety conjugated through the 13^1-carbon position upon exocyclic E-ring opening. Compound **4a** was synthesized from bacteriochlorophyll *a* and was used as the precursor for the synthesis of **1a**, **2a**, **3a**, **5a**, and **1b−5b**. The procedures used to synthesize bacteriochlorins **1a−5a** and **2b−5b** were facile and generally high-yielding. The spectroscopic properties, calculated molecular energies, and ROS photogeneration of **2a−5a** and **2b−5b** were then studied to elucidate structure−activity relationships as a result of taurine-driven exocyclic E-ring opening and net-charge variations.

Analysis of the absorbance spectra of **2a−5a** and **2b−5b** showed that taurine-driven exocyclic E-ring opening resulted in consistent hypsochromic shifts of the Q_x bands of **2b−5b** compared to **2a−5a**. Proton NMR analysis showed a consistent increase in the shielding of the H23-NH protons of **2b−5b** compared to **2a−5a**. This suggests that taurine-driven exocyclic

dx.doi.org/10.1021/jm401538h | J. Med. Chem. XXXX, XXX, XXX−XXX

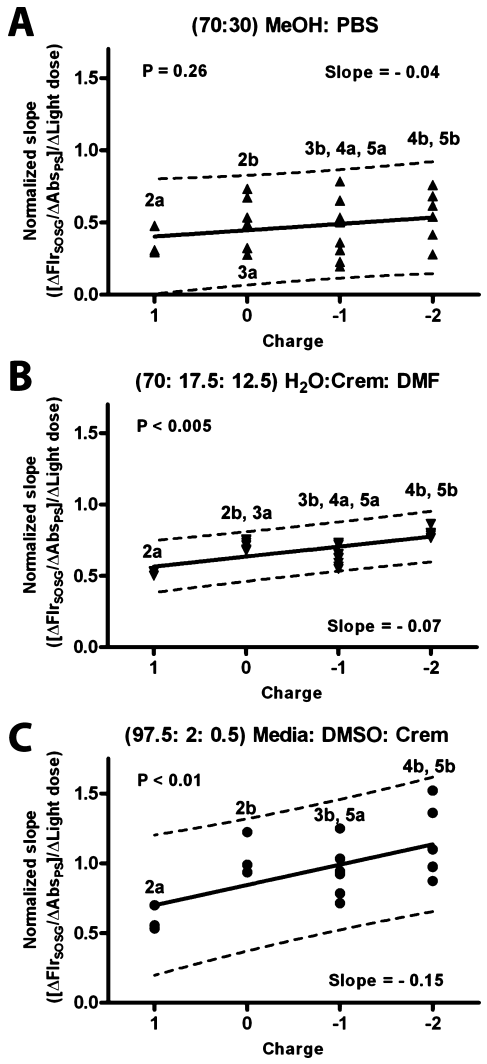

Figure 6. Photogeneration of ROS by bacteriochlorins indicated by linear slopes of corrected SOSG fluorescence ($\Delta Flr_{SOSG}/\Delta Abs_{PS}$; normalized to **1b**) over the light dose range (ΔLight dose) after 740 nm irradiation in MeOH-based solution (A; light dose = 0−250 mJ, $r^2 > 0.9978$), in H_2O with high detergent concentrations (B; light dose = 0−1000 mJ, $r^2 > 0.9827$), and in cell culture media (C; light dose = 0−750 mJ, $r^2 > 0.9846$) compared to the net charge of derivatives with (**2a**−**5a**) and without (**2b**−**5b**) the exocyclic E ring ($n = 3$, dashed lines show predicted 95% CI). Compounds **3a** and **4a** were excluded from assays in cell culture media (C) because of their observed aggregation (Figure S37).

E-ring opening resulted in enhancing the local electron density at the C ring of **2b**−**5b** compared to the C ring adjacent to the coplanar ketone moiety within the exocyclic E ring of **2a**−**5a**. We propose that these local electron-density enhancements modulated the aromatic-ring current of compounds **2b**−**5b**. DFT-based molecular modeling was then used to calculate the energy gaps between the HOMO−1 and LUMO energy levels because this energy gap reflects the relative maximum wavelength of the Q_x absorption bands of free-base bacteriochlorins.[27] These calculations showed that taurine-driven exocyclic E-ring opening consistently increased the HOMO−1-to-LUMO energy gaps of **2b**−**5b** compared to **2a**−**5a**. Therefore, we propose that taurine-driven exocyclic E-ring opening was responsible for the hypsochromic shifts of the Q_x absorption bands of **2b**−**5b** compared to **2a**−**5a** as a result of the enhanced local electron densities of the adjacent C rings of **2b**−**5b**. Although these ^{1}H NMR and DFT studies explain the distinct absorbance spectral shifts of **2b**−**5b** compared to **2a**−**5a**, we cannot directly suggest how variations in the local electron densities at the C ring of **2b**−**5b** can modulate the photophysical properties of **2a**−**5a**. However, an analogous investigation by Monteiro et al. concluded that electron-withdrawing substituents can reduce the Φ_T of *meso*-tetraphenyl-substituted free-base bacteriochlorins.[73] Ding et al. presented a similar report of enhancements of type 1 PDT ROS photogeneration by *meso*-tetra(hydroxyphenyl) porphyrin because of the encapsulation of the porphyrin within electron-donating micelles.[74] The summary of these observations suggest that the inclusion of electron-donating groups and the avoidance of electron-withdrawing groups may potentially enhance the photogeneration of type 1 and/or type 2 PDT ROS of bacteriochlorins.

The ΔE^{ST} of **2a**−**5a** and **2b**−**5b** were calculated to predict theoretically if these bacteriochlorins would be capable of generating $^1O_2$ via type 2 PDT using TDDFT molecular modeling. The results showed that each bacteriochlorin had the potential to generate $^1O_2$ by transferring their triplet excited-state energy to triplet ground-state molecular oxygen ($^3O_2$). In addition, because the ΔE^{ST} energies were greater for **2b**−**5b** compared to corresponding **2a**−**5a**, we predicted that taurine-driven exocyclic E-ring opening could potentially modulate the photogeneration of ROS. Analysis of our experimental PDT ROS studies found that taurine-driven exocyclic E-ring opening (**2b**−**5b** vs **2a**−**5a**) consistently enhanced the photogeneration of ROS in each of the tested solutions using both AUR- and SOSG-based analysis. In light of our ROS-specificity studies and because of the known capture of interrelated type 1 PDT ROS[7] by AUR[48−52] and SOSG,[72] we propose that a combination of superoxide, hydrogen peroxide, hydroxyl radicals, and $^1O_2$ were detected during our ROS assays. We observed the most consistent ROS photogeneration enhancements for **2b**, **4b**, and **5b** compared to **2a**, **4a** and **5a**, respectively. The largest enhancements of ROS photogeneration was observed with **2b** compared to **2a** (AUR- and SOSG-based studies) in all of the tested solutions. Our structure−activity relationships corroborate a report by Joshi et al. that showed that exocyclic E-ring opening consistently enhanced the in vitro PDT activity of three pairs of neutral free-base bacteriochlorins containing ketone functional groups either at the B ring or the D ring.[75] In light of our experimental PDT ROS results, it is possible that the in vitro PDT-activity enhancements described by Joshi et al. were the result of enhanced ROS photogeneration because of exocyclic E-ring opening. These findings suggest that exocyclic E-ring opening may generally enhance the ROS photogeneration of free-base bacteriochlorins to improve, potentially, in vitro PDT activity.

The palladium-containing controls, **1a** and **1b**, also showed an interesting trend wherein **1b** generated higher levels of ROS compared to **1a** in aqueous-based solutions but not in the MeOH-based solution. It was previously shown that **1a** efficiently produces $^1O_2$ in organic solution,[17] whereas **1b** primarily produces superoxide and hydroxyl radicals in aqueous media.[24] The formation of $^1O_2$ via type 2 PDT is limited by the presence of dissolved and diffusing ground-state molecular O_2.[8,9] The type 1 PDT mechanisms, however, can involve electron transfer to molecular O_2 to form superoxide, which can continued to react with H_2O to form hydrogen peroxide.[7] Therefore, the ROS generation of **1b** was higher compared to

dx.doi.org/10.1021/jm401538h | J. Med. Chem. XXXX, XXX, XXX−XXX

1a in aqueous-based solutions in our report, likely because of the increased photogeneration of type 1 PDT ROS by **1b** through a cascade of reactions involving both O_2 and H_2O in the aqueous-based solutions.[7]

Our analysis also showed that varying the charge of the bacteriochlorins influenced the photogeneration of ROS, whereby an increasing net negative charge consistently resulted in an increased photogeneration of ROS in the aqueous-based solutions (AUR- and SOSG-based studies). Silva et al. have previously identified the sulfonic acid functional groups of the *meso*-tetra(2,6-dichloro-3-sulfonatophenyl) bacteriochlorin ($TDCPBSO_3H$) as the key sites of excited-state electron transfer for type 1 PDT.[76] This finding suggests that the sulfonic acid functional group of taurine on **5a** and **2b**−**5b** and possibly the carboxylic acid functional groups of compounds **4a** and **4b** were involved during excited-state electron transfer to generate type 1 PDT ROS. Therefore, we propose that the anionic functional groups of **4a**, **5a**, and **2b**−**5b** were influential for enhancing ROS photogeneration compared to the cationic compound, **2a**, in aqueous solutions.

We calculated the theoretical potential for type 2 PDT ROS generation of **2a**−**5a** and **2b**−**5b** and observed experimentally the variations in ROS photogeneration by these PSs. Although we observed that taurine-driven exocyclic E-ring opening and increasing the net negative charge enhanced ROS photogeneration, we cannot conclude the effects these structural modifications had on the photophysical properties of **2a**−**5a** and **2b**−**5b**. However, because taurine-driven exocyclic E-ring opening had little effect on the Φ_f and the Stokes shifts of **2a**−**5a** compared to **2b**−**5b**, we can infer that the observed variations of ROS photogeneration were likely the result of modulations of the quantum yields of intersystem crossing (Φ_{ISC}), Φ_T, and/or singlet oxygen formation (Φ_Δ) but not because of major differences in Φ_{IC}.[42−47] Extensive studies involving ESR analysis, transient absorption spectroscopy, and $^1O_2$ luminescence would further elucidate the role taurine-driven exocyclic E-ring opening and charge variations have on the photophysical properties of bacteriochlorins to conclude truly how our aforementioned structural modifications resulted in enhancements of ROS photogeneration. Such experiments could continue to refine structure−activity relationships that would facilitate the design of novel bacteriochlorin PSs for efficient type 1 and type 2 PDT.

CONCLUSIONS

We synthesized a series of eight free-base bacteriochlorophyll *a* derivatives to develop simple strategies for enhancing the photogeneration of ROS. TDDFT molecular modeling calculations predicted that each derivative would potentially generate $^1O_2$ upon photoirradiation. Further experimental investigations validated these predictive calculations and found that taurine-driven exocyclic E-ring opening and increasing net negative charge generally enhanced ROS photogeneration in aqueous solutions. These structure−activity relationships are meant to aid current PDT research by providing simple strategies to design novel bacteriochlorins that may efficiently generate type 1 and type 2 PDT ROS. These strategies may be particular useful when the type 1 PDT mechanism is required for anticancer or antimicrobial PDT applications under hypoxic or anoxic conditions.

EXPERIMENTAL SECTION

Materials. Bacterial cultures of *R. sphaeroides* were purchased from Frontier Scientific Inc. The reagents taurine, sodium ascorbate, palladium acetate, choline chloride, *N*,*N*′-dicyclohexylcarbodiimide (DCC), *O*-benzotriazole-*N*,*N*,*N*′,*N*′-tetramethyl-uronium-hexafluorophosphate (HBTU), 4-(*N*,*N*-dimethylamino)pyridine (DMAP), and *N*,*N*-diisopropylethylamine (DIPEA) were purchased from Sigma-Aldrich and used without further purification. Deuterated NMR solvents, DMSO-d_6 and $CDCl_3$, were purchased from Cambridge Isotope Laboratories. The ROS-activated fluorescent probes Amplex UltraRed (AUR) and Singlet Oxygen Sensor Green (SOSG) were purchased from Invitrogen. The ROS quenchers, *N*,*N*′-dimethyl thiourea (DMTU), 1,2-dihydroxybenzene-3,5-disulfonic acid disodium salt hydrate (tiron), and sodium azide, were purchased from Sigma-Aldrich and used without further purification. The MTT reagent (3-(4,5-dimethylthiazol-2-yl)-2,5-diphenyltetrazolium bromide) was purchased from Invitrogen-Gibco.

Chemistry. *General Information.* All synthetic reactions were performed in round-bottomed flasks sealed with rubber septa using magnetic stirring under either Ar(g) or N_2(g). Rotary evaporation was performed while heating solutions at 40 °C and appropriately adjusting vacuum pressures for various solvents. Normal-phase column chromatography was performed during the synthesis of **4a** using Merck grade 60 silica gel (70−230 mesh size, 60 Å). Compounds **2a**, **3a**, **5a**, and **2b**−**5b** were purified using a Biotage Isolera One flash chromatography system with a 25 g Biotage C-18 cartridge under reverse-phase conditions (gradient of 0−100% ACN in 0.1% TFA over 12 min using a flow of 40 mL/min) while monitoring eluted products at 357 nm and byproducts at 200 nm. Compound **1b** was initially purified with the aforementioned Biotage system under reverse-phase conditions (gradient 0−100% ACN in 5 mM K_2HPO_4(aq) over 12 min using a flow of 40 mL/min) while monitoring the eluted product at 383 nm and was further purified using a Waters 2695 HPLC with a 25 cm C-18 column under reverse-phase conditions (gradient of 20−100% ACN with 0.1 M TEAA(aq) over 40 min using a flow of 0.5 mL/min) while monitoring the eluted fractions of **1b** (λ_{abs} = 517 and 750 nm) and the chlorin analogue of **1b** (λ_{abs} = 628 nm) using a Waters 2996 photodiode array detector (200−800 nm). The identity and purity of all compounds (**1a**−**5a** and **1b**−**5b**) was assessed using the aforementioned HPLC system with a Waters Delta Pak C18, 5 μm 3.9 × 150 mm column under reverse-phase conditions (gradient of 0−100% acetonitrile in 0.1% TFA over 15 min using a flow of 0.8 mL/min) while monitoring eluted samples with the aforementioned photodiode array detector (λ_{abs} = 750 nm) and a Waters Micromass ZQ mass spectrometer (200−2000 m/z) in ESI-positive mode. HPLC−MS analysis showed that all compounds were ≥95% pure. The identity of **1a**−**5a** and **2b**−**5b** was also assessed by 1D ^{1}H NMR, 2D COSY ^{1}H NMR, and ^{13}C Jmod NMR analysis using a Bruker Ultrashield 400 Plus 400 MHz NMR with either DMSO-d_6 or $CDCl_3$. ^{1}H NMR analysis showed that compounds were ≥95% pure unless stated otherwise (**3b** and **4a**). The solubility of all compounds (in PBS with 2.0% DMSO (v/v) and 0.5% cremophor (v/v)) was assessed using a Varian 50 Bio UV−vis spectrophotometer. The fluorescence spectra of all bacteriochlorins were recorded in MeOH using a Horiba Jobin Yvon Fluoromax-4 spectrofluorometer. The comparative ROS photogeneration assays involved irradiating all compounds using a 740 nm LED light box and recording absorbance values and fluorescence intensities using a Molecular Devices Spectra Max M5 plate reader.

*Palladium Bacteriopheophorbide a (**1a**).* Compound **1a** was synthesized according to literature procedures.[12] The precursor, **4a** (70 mg, 114.8 μmol or 1.0 equiv), and $Pd(OAc)_2$ (56 mg, 252.6 μmol or 2.2 equiv) were dissolved in 42 mL of (1:5) DCM/MeOH. Sodium ascorbate (140 mg, 711.8 μmol or 6.2 equiv) was suspended in the solution, and the mixture was purged with Ar(g) for 2 min. The mixture was then stirred in the dark at room temperature overnight. Chloroform (40 mL) was added, and the mixture was washed four times with 30 mL of saturated NaCl(aq). The organic layer was then dried using Na_2SO_4, filtered, and concentrated by rotary evaporation. The crude product was redissolved in 42 mL of 1:5 DCM/MeOH, and

dx.doi.org/10.1021/jm401538h | J. Med. Chem. XXXX, XXX, XXX−XXX

the previously described amounts of $Pd(OAc)_2$ and sodium ascorbate were added. The mixture was then stirred at room temperature in the dark overnight. The same extraction was repeated, and the same reaction conditions and extraction was performed a total of five times. This yielded 56.7 mg (79.4 μmol) of **1a** (69% yield). ESI+MS: $[M + H]^+$ = 715 *m/z*. UV−vis (MeOH, λ_{max}): 756, 533, 383, 329 nm. ^{1}H NMR (400 MHz, $CDCl_3$): δ 9.21 (s, 1H, 5H), 8.52 (s, 1H, 10H), 8.47 (s, 1H, 20H), 5.93 (s, 1H, 13^2H), 4.38 (m, 1H, 18H), 4.36 (m, 1H, 7H), 4.08 (m, 2H, 17H + 8H), 3.87 (s, 3H, 12^1CH_3), 3.46 (s, 3H, 15^3OCH_3), 3.38 (s, 3H, 2^1CH_3), 3.08 (s, 3H, 3^2COCH_3), 2.52 (m, 2H, $17a^2CH_2$), 2.35 (m, 2H, $17b^1H$ + $17a^2H$), 2.20 (m, 2H, $17b^2H$ + $8a^1H$), 2.07 (m, 1H, $8b^1H$), 1.77 (d, 3H, *J* = 7.2 Hz, 18^1CH_3), 1.67 (d, 3H, *J* = 7.0 Hz, 7^1CH_3), 1.07 (t, 3H, *J* = 7.3 Hz, 8^2CH_3). ^{13}C NMR (100 MHz, $CDCl_3$): δ 198.21, 187.56, 169.57, 159.13, 158.02, 151.05, 150.03, 144.69, 141.33, 140.71, 140.01, 136.24, 134.87, 129.70, 126.60, 126.41, 109.22, 102.32, 100.94, 98.05, 64.38, 54.34, 52.85, 48.58, 46.77, 34.34, 32.88, 32.13, 30.12, 23.23, 23.19, 20.84, 13.98, 12.11, 10.26.

*Palladium 3^1-Oxo-15-methoxycarbonylmethyl-rhodobacteriochlorin 13′-(2-Sulfethyl)amide (**1b**).* The precursor, **1a** (24.7 mg, 34.5 μmol or 1.0 equiv), was dissolved in 3.7 mL of DMSO. DCC (50.3 mg, 241.8 μmol or 7.0 equiv) and DMAP (14.8 mg, 241.8 μmol or 7.0 equiv) were then dissolved in the DMSO solution. A 1.235 mL solution was prepared using 34.5 mg (274.3 μmol or 7.94 equiv) of taurine in 1 M K_2HPO_4(aq) with a pH of 8.2 according to literature procedures.[18,19] The solutions were combined, and the resulting suspension was stirred in the dark at room temperature for 4 days while constantly bubbling N_2(g). The crude product was purified using a reverse-phase Biotage system. The collected fraction (eluted at ∼50% ACN (v/v)) was concentrated by rotary evaporation and dried using a speed-vac. The dried crude product was dissolved in 200 μL of DMSO and purified by reverse-phase HPLC. The product was quantified spectrophotometrically, the identity was characterized using ESI+MS and UV−vis spectroscopy, and the purity was found to be >95% using HPLC−MS. This yielded 0.21 mg (250 nmol) of **1b** (0.7% yield). ESI+MS: $[M]^+$ = 840 *m/z*. UV−vis (MeOH, λ_{max}): 748, 517, 385, 332 nm.

*3^1-Oxo-rhodobacteriochlorin 17^3-(2-Trimethylaminoethyl)ester (**2a**).* Compound **2a** was synthesized according to literature procedures.[39] The precursor, **4a** (70 mg, 114.8 μmol or 1.0 equiv), was dissolved in 3.4 mL of DMSO. HBTU (88.9 mg, 229.6 μmol or 2.0 equiv), DMAP (29.9 mg, 229.6 μmol or 2.0 equiv), and DIPEA (99.2 μL, 574 μmol or 5.0 equiv) were then added to the DMSO solution. Choline chloride (63 mg, 574 μmol or 5.0 equiv) was dissolved in 63 μL of H_2O and was added to the DMSO solution. The mixture was purged with Ar(g) for 2 min and was stirred in the dark at room temperature for 117 h. The crude product was then purified using a reverse-phase Biotage system. The collected fraction (eluted at ∼75% ACN (v/v)) was concentrated by rotary evaporation and dried using a speed-vac. This yielded 11 mg (15.7 μmol) of product **2a** (14% yield). ESI+MS: $[M + H]^+$ = 698 *m/z*. UV−vis (MeOH, λ_{max}): 745, 527, 357 nm. ^{1}H NMR (400 MHz, DMSO-d_6): δ 8.95 (s, 1H, 5H), 8.72 (s, 1H, 10H), 8.66 (s, 1 H, 20H), 6.14 (s, 1H, 13^2H), 4.35 (m, 2H, choline CH_2), 4.33 (m, 1H, 7H), 4.27 (m, 1H, 18H), 4.01 (m, 1H, 8H), 3.81 (m, 1H, 17H), 3.76 (s, 3H, 12^1CH_3), 3.53 (m, 2H, choline CH_2), 3.47 (s, 3H, 15^3OCH_3), 3.33 (s, 3H, 2^1CH_3), 3.13 (s, 3H, 3^2COCH_3), 2.98 (s, 9H, choline $3CH_3$) 2.32 (m, 1H, 8^1CH), 2.30 (m, 2H, 17^1H), 2.18 (m, 2H, 17^2H), 2.03 (m, 1H, 8^1CH), 2.01 (m, 2H, 17^1H), 1.72 (d, 3H, *J* = 7.1 Hz, 18^1CH_3), 1.66 (d, 3H, *J* = 7.1 Hz, 7^1CH_3), 1.00 (t, 3H, *J* = 7.3 Hz, 8^2CH_3), 0.70 (s, 1H, 23-NH), −0.82 (s, 1H, 21-NH). ^{13}C NMR (100 MHz, DMSO-d_6): δ 199.39, 188.93, 172.36, 172.01, 171.54, 169.67, 163.73, 157.83, 147.81, 139.02, 138.47, 137.35, 133.67, 128.14, 120.02, 108.51, 100.00, 97.44, 97.15, 64.26, 64.11, 58.29, 54.28, 53.29, 53.09, 50.34, 49.37, 48.55, 40.68, 33.69, 30.81, 29.86, 29.17, 23.11, 22.92, 13.40, 11.47, 10.90.

*3^1-Oxo-15-methoxycarbonylmethyl-rhodobacteriochlorin-13^1-(2-sulfethyl)amide-17^3-(2-trimethylaminoethyl)ester (**2b**).* The precursor, **4b** (39.2 mg, 53.2 μmol or 1.0 equiv), was dissolved in 11.2 mL of ACN. HBTU (41.7 mg, 106.4 μmol or 2.0 equiv), DMAP (19.7 mg, 106.4 μmol or 2.0 equiv), and DIPEA (91.9 μL, 127.5 μmol or 10.0 equiv) were then added to the ACN solution. Choline chloride (29.2 mg, 266 μmol or 5.0 equiv) was dissolved in 29 μL of H_2O and was added to the ACN solution. The solution was purged with Ar(g) for 1 min and stirred in the dark at room temperature for 20 h. The crude product was then purified using a reverse-phase Biotage system. The collected fraction (eluted at ∼60% ACN (v/v)) was concentrated by rotary evaporation and dried using a speed-vac. This yielded 20 mg (24.3 μmol) of product **2b** (46% yield). ESI+MS: $[M]^+$ = 822 *m/z*. UV−vis (MeOH, λ_{max}): 749, 517, 354 nm. ^{1}H NMR (400 MHz, DMSO-d_6): δ 9.30 (s, 1H, 5H), 8.93 (s, 1H, 10H), 8.90 (s, 1H, taurine NH), 8.77 (s, 1 H, 20H), 5.34 (d, 1H, *J* = 19.3 Hz, $14a^2$H), 5.13 (d, 1H, *J* = 17.3 Hz, $14b^2$H), 4.39 (m, 2H, choline CH_2), 4.35(m, 1H, 7H), 4.33 (m, 1H, 18H), 4.22 (m, 1H, 17H), 4.20 (m, 1H, 18H), 3.80 (m, 2H, taurine CH_2), 3.65 (s, 3H, 12^1CH_3), 3.58 (s, 3H, 15^3OCH_3), 3.57 (m, 2H, choline CH_2), 3.24 (s, 3H, 2^1CH_3), 3.16 (s, 3H, 3^2COCH_3), 3.02 (s, 9H, choline $3CH_3$), 2.92 (m, 2H, taurine CH_2), 2.66 (m, 1H, $17a^2$H), 2.41 (m, 1H, $17b^2$H), 2.33 (m, 1H, 8^1CH), 2.06 (m, 1H, $17a^1$H), 2.04 (m, 1H, 8^1H), 1.80 (d, 3H, *J* = 6.9 Hz, 7^1CH_3), 1.55 (d, 3H, *J* = 6.8 Hz, 18^1CH_3), 1.49 (m, 1H, $17b^1$H), 0.99 (t, 3H, *J* = 7.3 Hz, 8^2CH_3), −1.32 (s, 2H, 21-NH + 23-NH). ^{13}C NMR (100 MHz, DMSO-d_6): δ 198.43, 173.00, 172.62, 167.70, 167.63, 167.19, 166.28, 163.42, 134.37, 134.04, 132.22, 131.73, 131.57, 131.32, 128.02, 105.25, 98.24, 97.96, 96.57, 64.04, 58.32, 57.02, 53.30, 53.00, 52.40, 50.76, 47.18, 46.10, 37.15, 33.56, 30.99, 29.68, 29.36, 24.01, 23.58, 13.73, 11.82, 10.90.

*3^1-Oxo-rhodobacteriochlorin 17^3-Methyl Ester (**3a**).* The precursor, **4a** (40 mg, 65.6 μmol or 1.0 equiv), was dissolved in 5 mL of DMSO. HBTU (51.4 mg, 131.2 μmol or 2.0 equiv) and DMAP (25.7 mg, μmol or 2.0 equiv) were then dissolved in the DMSO solution. Methanol (10 mL) was added to the DMSO solution, and the reaction was stirred in the dark for 3 h while gently bubbling N_2(g). The crude product was then purified using a reverse-phase Biotage system. The collected fraction (eluted at 100% ACN (v/v)) was concentrated by rotary evaporation and dried using a speed-vac. This yielded 14 mg (22.4 μmol) of product **3a** (34% yield). ESI+MS: $[M + H]^+$ = 625 *m/z*. UV−vis (MeOH, λ_{max}): 748, 527, 357 nm. ^{1}H NMR (400 MHz, $CDCl_3$): δ 8.99 (s, 1H, 5H), 8.50 (s, 1H, 10H), 8.43 (s, 1 H, 20H), 6.10 (s, 1H, 13^2H), 4.31 (m, 1H, 18H), 4.28 (m, 1H, 7H), 4.04 (m, 1H, 17H), 4.03 (m, 1H, 8H), 3.86 (s, 3H, 12^1CH_3), 3.61 (s, 3H, 15^3OCH_3), 3.51 (s, 3H, 2^1CH_3), 3.46 (s, 3H, 3^2COCH_3), 3.18 (s, 3H, 17^4OCH_3), 2.51 (m, 2H, 17^2CH_2), 2.34 (m, 1H, 8^1H), 2.26 (m, 1H, $17a^1$H), 2.08 (m, 1H, $17b^1$H), 2.06 (m, 1H, 8^1H), 1.80 (d, 3H, *J* = 7.1 Hz, 18^1CH_3), 1.74 (d, 3H, *J* = 7.2 Hz, 7^1CH_3), 1.12 (t, 3H, *J* = 7.3 Hz, 8^2CH_3), 0.48 (s, 1H, 23NH), −0.95 (s, 1H, 21NH). ^{13}C NMR (100 MHz, $CDCl_3$): δ 199.10, 189.04, 173.31, 171.04, 169.53, 163.65, 157.92, 148.09, 139.07, 138.29, 136.83, 136.25, 133.28, 128.66, 121.36, 108.03, 99.62, 97.64, 95.78, 64.35, 54.97, 52.78, 51.67, 50.61, 49.71, 48.87, 33.32, 30.95, 30.16, 29.93, 22.91, 22.85, 13.40, 11.51, 10.75.

*3^1-Oxo-15-methoxycarbonylmethyl-rhodobacteriochlorin 13′-(2-Sulfethyl)amide-17^3-methyl Ester (**3b**).* The precursor, **4b** (20 mg, 27.1 μmol or 1.0 equiv), was dissolved in 2 mL of DMSO. HBTU (21 mg, 54.3 μmol or 2.0 equiv) and DMAP (6.5 mg, 54.3 μmol or 2.0 equiv) were dissolved in the DMSO solution. Methanol (2 mL) was added to the DMSO solution, and the mixture was purged with Ar(g) for 2 min and stirred in the dark for 21 h. The crude product was then purified using a reverse-phase Biotage system. The collected fraction (eluted at ∼70% ACN (v/v)) was concentrated by rotary evaporation and dried using a speed-vac. This yielded 12 mg (16 μmol) of product **3b** (59% yield). Compound **3b** was assessed to be ∼94% pure by ^{1}H NMR analysis. ESI+MS: $[M + H]^+$ = 751 *m/z*. UV−vis (MeOH, λ_{max}): 749, 517, 356 nm. ^{1}H NMR (400 MHz, DMSO-d_6): δ 9.30 (s, 1H, 5H), 8.93 (s, 1H, 10H), 8.91 (s, 1H, taurine NH), 8.76 (s, 1H, 20H), 5.31 (d, 1H, *J* = 18.7 Hz, $14a^2$H), 5.14 (d, 1H, *J* = 18.5 Hz, $14b^2$H), 4.33 (m, 1H, 7H), 4.31 (m, 1H, 18H), 4.22 (m, 1H, 17H), 4.17 (m, 1H, 8H), 3.79 (m, 2H, taurine CH_2), 3.65 (s, 3H, 12^1CH_3), 3.58 (s, 3H, 15^3OCH_3), 3.56 (s, 3H, 17^4OCH_3), 3.24 (s, 3H, 2^1CH_3), 3.16 (s, 3H, 3^2COCH_3), 2.92 (m, 2H, taurine CH_2), 2.63 (m, 1H, $17a^2$H), 2.61 (m, 1H, $17b^2$H), 2.40 (m, 1H, $17a^1$H), 2.32 (m, 1H, 8^1CH), 2.06 (m, 1H, 8^1H), 2.03 (m, 1H, $17b^1$H), 1.81 (d, 3H, *J* = 7.0 Hz, 18^1CH_3), 1.53 (d, 3H, *J* = 6.8 Hz, 7^1CH_3), 0.99 (t, 3H, *J* = 7.2 Hz,

dx.doi.org/10.1021/jm401538h | J. Med. Chem. XXXX, XXX, XXX−XXX

8^2CH_3), −1.31 and −1.32 (each s, 21NH + 23NH). ^{13}C NMR (100 MHz, DMSO-d_6): δ 198.43, 173.58, 172.99, 167.68, 167.65, 167.33, 166.18, 163.49, 134.36, 134.05, 134.01, 132.13, 131.72, 131.57, 131.36, 128.00, 105.29, 98.28, 97.91, 96.50, 57.04, 53.12, 52.32, 51.77, 50.84, 47.18, 46.10, 37.12, 33.79, 33.55, 30.94, 29.66, 29.40, 24.00, 23.50, 13.73, 11.78, 10.89.

*Bacteriopheophorbide a (**4a**).* Compound **4a** was synthesized according to literature procedures[37,38] and was used as the precursor for the synthesis of all other bacteriochlorins in this study. A 450 mL volume of *R. sphaeroides* was processed to yield 942 mg (1.54 mmol) of **4a**. HPLC−MS analysis showed one distinct eluted product with the corresponding [M + H] value of **4a** (Figure S12), whereas ^1H NMR revealed the presence of a stereoisomer of **4a** (∼ 10%) with shifts of 7^1H, 8^2H, 13^2H, 18^1H at chiral positions (Figure S9). ESI +MS: $[M + H]^+$ = 611 *m*/*z*. UV−vis (MeOH, λ_{max}): 744, 527, 357 nm. ^1H NMR (400 MHz, DMSO-d_6): δ 8.95 (s, 1H, 5H), 8.72 (s, 1H, 10H), 8.63 (s, 1 H, 20H), 6.17 (s, 1H, 13^2H), 4.34 (m, 1H, 7H), 4.25 (m, 1H, 18H), 3.99 (m, 1H, 8H), 3.82 (m, 1H, 17H), 3.79 (s, 3H, 12^1CH_3), 3.45 (s, 3H, 15^3OCH_3), 3.32 (s, 3H, 2^1CH_3), 3.11 (s, 3H, 3^2COCH_3), 2.35 (m, 3H, $17a^2H$ + 8^1CH_2), 2.18 (m, 1H, $17b^2H$), 2.03 (m, 2H, 17^1CH_2), 1.71 (d, 3H, *J* = 6.9 Hz, 18^1CH_3), 1.64 (d, 3H, *J* = 7.0 Hz, 7^1CH_3), 1.02 (t, 3H, *J* = 6.8 Hz, 8^2CH_3), 0.65 (s, 1H, 23NH), −0.85 (s, 1H, 21NH). ^{13}C NMR (100 MHz, DMSO-d_6): δ 199.37, 188.97, 174.43, 171.82, 171.55, 169.71, 163.64, 158.37, 147.85, 138.89, 138.45, 138.40, 137.28, 133.53, 128.13, 119.98, 108.67, 99.87, 97.30, 97.24, 64.23, 54.32, 53.03, 50.52, 49.42, 48.53, 33.66, 31.06, 29.84, 29.52, 23.10, 22.99, 13.39, 11.46, 10.89.

*3^1-Oxo-15-methoxycarbonylmethyl-rhodobacteriochlorin 13′-(2-Sulfethyl)amide (**4b**).* The precursor, **4a** (80 mg, 131.2 μmol or 1.0 equiv), was dissolved in 12 mL of DMSO. DCC (190.4 mg, 918.4 μmol or 7.0 equiv) and DMAP (56 mg, 918.4 μmol or 7.0 equiv) were then dissolved in the DMSO solution. A 4 mL solution was prepared using 131.2 mg (1.042 mmol or 7.94 equiv) of taurine in 1 M K_2HPO_4(aq) with a pH of 8.2 according to literature procedures.[18,19] The solutions were mixed, and the resulting suspension was stirred in the dark at room temperature for 10 days with constant gentle N_2(g) bubbling. The crude product was then purified using a reverse-phase Biotage system. The collected fraction (eluted at ∼70% ACN (v/v)) was concentrated by rotary evaporation and dried using a speed-vac. This yielded 36.2 mg (49.1 μmol) of product **4b** (37% yield). ESI +MS: $[M + H]^+$ = 737 *m*/*z*. UV−vis (MeOH, λ_{max}): 749, 518, 354 nm. ^1H NMR (400 MHz, DMSO-d_6): δ 9.30 (s, 1H, 5H), 8.93 (s, 1H, 10H), 8.93 (s, 1H, taurine NH), 8.75 (s, 1 H, 20H), 5.33 (d, 1H, *J* = 20.0 Hz, $14a^2H$), 5.22 (d, 1H, *J* = 18.1 Hz, $14b^2H$), 4.33 (m, 1H, 7H), 4.31(m, 1H, 18H), 4.21 (m, 1H, 17H), 4.20 (m, 1H, 8H), 3.76 (m, 2H, taurine CH_2), 3.65 (s, 3H, 12^1CH_3), 3.58 (s, 3H, 15^3OCH_3), 3.24 (s, 3H, 2^1CH_3), 3.15 (s, 3H, 3^2COCH_3), 2.93 (m, 2H, taurine CH_2), 2.54 (m, 1H, $17a^2H$), 2.39 (m, 2H, 8^1CH + $17b^2H$), 2.24 (m, 1H, $17a^1H$), 2.04 (m, 1H, $17b^1H$), 2.02 (m, 1H, 8^1H), 1.81 (d, 3H, *J* = 7.0 Hz, 18^1CH_3), 1.54 (d, 3H, *J* = 6.8 Hz, 7^1CH_3), 1.48 (m, 1H, 17^1H), 0.98 (t, 3H, *J* = 7.0 Hz, 8^2CH_3), −1.30 (s, 2H, 21NH + 23NH). ^{13}C NMR (100 MHz, DMSO-d_6): δ 198.43, 174.85, 173.05, 167.73, 167.67, 167.59, 166.22, 163.52, 134.40, 134.06, 134.01, 132.15, 131.77, 131.49, 131.30, 127.92, 105.38, 98.32, 97.89, 96.45, 57.04, 53.24, 52.30, 50.86, 47.20, 46.07, 37.13, 33.56, 32.66, 31.08, 29.66, 29.46, 24.01, 23.58, 13.74, 11.79, 10.90.

*3^1-Oxo-rhodobacteriochlorin 17^3-(2-Sulfethyl)amide (**5a**).* The precursor, **4a** (25 mg, 16.4 μmol or 1.0 equiv), was dissolved in 3.75 mL of DMSO. HBTU (111 mg, 286.1 μmol or 7.0 equiv) was then dissolved in the DMSO solution. A 1.25 mL solution was prepared using 41.2 mg (326.8 μmol or 8.0 equiv) of taurine in 1 M K_2HPO_4(aq) with a pH of 8.2 according to literature procedures.[18,19] The solutions were combined, and the resulting suspension was purged with Ar(g) for 2 min. The mixture was then stirred in the dark at 40 °C for 22 h. The crude product was then purified using a reverse-phase Biotage system. The collected fraction (eluted at ∼75% ACN (v/v)) was concentrated by rotary evaporation and dried using a speed-vac. This yielded 16 mg (22.2 μmol) of product **5a** (54% yield). ESI+MS: $[M + H]^+$ = 719 *m*/*z*. UV−vis (MeOH, λ_{max}): 747, 528, 357 nm, ^1H NMR (400 MHz, DMSO-d_6): δ 8.95 (s, 1H, 5H), 8.73 (s, 1H, 10H), 8.63 (s, 1 H, 20H), 7.62 (s, 1H, taurine NH), 6.17 (s, 1H, 13^2H), 4.31 (m, 1H, 7H), 4.26 (m, 1H, 18H), 3.99 (m, 1H, 8H), 3.79 (s, 3H, 12^1CH_3), 3.76 (m, 1H, 17H), 3.47 (s, 3H, 15^3OCH_3), 3.33 (s, 3H, 2^1CH_3), 3.24 (m, 2H, taurine CH_2), 3.12 (s, 3H, 3^2COCH_3), 2.71 (m, 2H, taurine CH_2), 2.44 (m, 2H, 17^1CH_2) 2.34 (m, 1H, 8^1CH), 2.10 (m, 1H, $17a^1H$), 2.02 (m, 1H, $17b^1H$), 1.97 (m, 1H, 8^1H), 1.72 (d, 3H, *J* = 7.3 Hz, 18^1CH_3), 1.64 (d, 3H, *J* = 6.8 Hz, 7^1CH_3), 1.01 (t, 3H, *J* = 7.3 Hz, 8^2CH_3), 0.68 (s, 1H, 23NH), −0.84 (s, 1H, 21NH). ^{13}C NMR (100 MHz, DMSO-d_6): δ 199.38, 189.04, 171.766, 171.714, 171.573, 169.77, 163.59, 158.60, 147.87, 138.92, 138.477, 138.422, 137.28, 133.47, 128.12, 119.93, 108.62, 99.82, 97.32, 97.25, 64.17, 54.32, 53.02, 51.01, 50.81, 49.52, 48.52, 35.97, 33.66, 32.82, 30.33, 29.82, 23.10, 22.95, 13.41, 11.47, 10.90.

*3^1-Oxo-15-methoxycarbonylmethyl-rhodobacteriochlorin 13^1,17^3-Di(2-sulfethyl)amide (**5b**).* The precursor, **4b** (38.5 mg, 52.2 μmol or 1.0 equiv), was dissolved in 5.775 mL of DMSO. HBTU (138.7 mg, 365.7 μmol or 7.0 equiv) was then dissolved in the DMSO solution. A 1.925 mL solution was prepared using 51.9 mg (414.8 μmol or 7.94 equiv) of taurine in 1 M K_2HPO_4(aq) with a pH of 8.2 according to literature procedures.[18,19] The solutions were combined, and the resulting suspension was purged with Ar(g) for 2 min. The mixture was stirred in the dark at 40 °C for 19 h. The crude was then purified using a reverse-phase Biotage system (with a 25 g C-18 Biotage cartridge using a 20−40% ACN gradient in 0.1% TFA over 12 column volumes and a flow of 40 mL/min) while monitoring impurities at 200 nm and collecting the product by monitoring it at 357 nm. The collected fraction (eluted at ∼40% ACN (v/v)) was concentrated by rotary evaporation and dried using a speed-vac. This yielded 9.5 mg (10.7 μmol) of product **5b** (28% yield). ESI+MS: $[M + H]^+$ = 844 *m*/*z*. UV−vis (MeOH, λ_{max}): 750, 518, 353 nm. ^1H NMR (400 MHz, DMSO-d_6): δ 9.29 (s, 1H, 5H), 8.92 (s, 1H, 10H), 8.90 (s, 1H, taurine NH), 8.73 (s, 1 H, 20H), 7.82 (s, 1H, taurine NH), 5.31 (d, 1H, *J* = 18.6 Hz, $14a^2H$), 5.10 (d, 1H, *J* = 18.6 Hz, $14b^2H$), 4.31 (m, 1H, 7H), 4.21 (m, 1H, 18H), 4.08 (d, 1H, J = 9.5 Hz, 17H), 3.96 (m, 1H, 8H), 3.81 (m, 2H, taurine CH_2), 3.67 (s, 3H, 12^1CH_3), 3.58 (s, 3H, 15^3OCH_3), 3.32 (m, 2H, taurine CH_2), 3.24 (s, 3H, 2^1CH_3), 3.15 (s, 3H, 3^2COCH_3), 2.95 (m, 2H, taurine CH_2), 2.56 (m, 2H, taurine CH_2), 2.53 (m, 1H, $17a^2H$), 2.39 (m, 1H, $17b^2H$), 2.37 (m, 1H, 8^1CH), 2.04 (m, 1H, 8^1H), 2.02 (m, 2H, 17^1H), 1.81 (d, 3H, *J* = 7.1 Hz, 18^1CH_3), 1.54 (d, 3H, *J* = 6.9 Hz, 7^1CH_3), 0.99 (t, 3H, *J* = 7.2 Hz, 8^2CH_3), −1.27 and −1.28 (each s, 2H, 21NH + 23NH). ^{13}C NMR (100 MHz, DMSO-d_6): δ 198.44, 172.98, 171.85, 168.05, 167.72, 167.51, 166.19, 163.63, 134.42, 134.07, 133.98, 132.13, 131.68, 131.45, 131.30, 127.87, 105.34, 98.33, 97.87, 96.36, 57.06, 53.28, 52.33, 51.06, 50.87, 47.36, 46.07, 37.02, 35.98, 33.55, 32.95, 30.31, 29.65, 24.00, 23.56, 13.76, 11.79, 10.92.

ROS Photogeneration Detected with AUR and SOSG. The PSs were dissolved in 100 μL of 70:30 MeOH/PBS, 70:17.5:12.5 H_2O/cremophor/DMF, or 97.5:2:0.5 RPMI-1640 cell culture media/DMSO/cremophor on sterile black-sided, clear-bottomed Costar 96-well plates (*n* = 3 for each solution). Compounds **3a** and **4a** were excluded from assays in cell culture media because of their observed aggregation in 97.5% (v/v) aqueous solution containing 2.0% DMSO (v/v) and 0.5% cremophor (v/v) (Figure S37). Stock solutions of AUR (1 mg/340 μL DSMO) and SOSG (1 mg/220 μL DMF) were prepared, and 1 μL aliquots of either AUR or SOSG stock solutions were added to each of the wells (25 μM AUR/well or 25 μM SOSG/well) containing the PSs (with either AUR or SOSG alone as controls). The absorbance of each sample was recorded at 740 nm to ensure the absorbance of all wells were matched (OD_{740} = 0.2) after blanking (using AUR or SOSG alone as baseline). The fluorescence of AUR (λ_{ex} = 550 nm; λ_{em} = 581 nm) and SOSG (λ_{ex} = 485 nm; λ_{em} = 536 nm) was then recorded to determine the baseline intensities of AUR and SOSG. Plates were then irradiated with a 740 nm LED light box (12.2 mW/cm^2 fluence rate). After irradiation, the absorbance of all samples was again recorded at 740 nm to determine the relative amount of PSs (ΔAbs_{PS})[61−64] remaining after photobleaching by the generated PDT ROS.[77−81] The fluorescence of AUR and SOSG was concomitantly recorded to determine the increase of activated AUR and SOSG resulting from the trapping of ROS generated by the

dx.doi.org/10.1021/jm401538h | J. Med. Chem. XXXX, XXX, XXX−XXX

irradiated PSs. These fluorescence values were then blanked according to the baseline fluorescence of AUR and SOSG to determine the increasing fluorescence of AUR (ΔFIr_{AUR}) and SOSG (ΔFIr_{SOSG}) for each light dose treatment. Because both the photobleaching of the PSs[62,80,81] and the increased fluorescence intensities of the ROS indicators illustrate the relative amounts of ROS that were generated during the irradiation of the PSs, these two metrics were combined to express the relative ROS photogeneration as the slopes of increasing corrected ROS-indicator fluorescence ($\Delta FIr_{SOSG/AUR}/\Delta Abs_{PS}$) over the light dose range (ΔLight dose) according to literature methods.[63−66] These slopes were normalized to the slope of the control, **1b**, in each of the tested solutions to illustrate the relationship between relative ROS photogeneration and net-charge variations.

Computational Studies. The DFT methods were implemented in SPARTAN 06 (Wave function Inc., Irvine, CA). The compounds were first geometry-optimized at the DFT level using the B3LYP functional and 6-31G* basis set,[25,26] with no symmetry restrictions and in the gas phase.[28,29] From these calculations, the energy levels for all compounds were extracted.[26] Following this, symmetry-unrestricted, gas-phase TDDFT single-point energy calculations were performed for the triplet excited state using the ground-state-optimized geometry. The vertical excitation energies for the compounds were obtained from this calculation.[28−30,33−36]

■ ASSOCIATED CONTENT

Supporting Information

NMR and HPLC−MS spectra, calculated energy levels and vertical excitation energies, AUR and SOSG specificity assays, cell viability relative to detergent concentrations, and absorbance-based solubility results. This material is available free of charge via the Internet at http://pubs.acs.org.

■ AUTHOR INFORMATION

Corresponding Author

*Tel: 416-581-7666. Fax 416-581-7667. E-mail: gzheng@uhnresearch.ca.

Notes

The authors declare no competing financial interest.

■ ACKNOWLEDGMENTS

This work was supported by the Natural Sciences and Engineering Research Council of Canada, Canadian Institute of Health Research, Canadian Cancer Society Research Institute, Canadian Foundation for Innovation, Joey and Toby Tanenbaum/Brazilian Ball Chair in Prostate Cancer Research, and Princess Margaret Cancer Foundation.

■ ABBREVIATIONS USED

ACN, acetonitrile; AUR, Amplex UltraRed; CI, confidence interval; COSY, correlation spectroscopy; Crem, cremophor; DCC, *N*,*N*′-dicyclohexylcarbodiimide; DCM, dichloromethane; DFT, density functional theory; DIPEA, *N*,*N*-diisopropylethylamine; DMAP, 4-(*N*,*N*-dimethylamino)pyridine; DMF, dimethylformamide; DMSO, dimethyl sulfoxide; DMTU, *N*,*N*′-dimethyl thiourea; ESI, electrospray ionization; ESR, electron spin resonance; HBTU, *O*-benzotriazole-*N*,*N*,*N*′,*N*′-tetramethyl-uronium-hexafluoro-phosphate; HOMO, highest occupied molecular orbital; HPLC, high-performance liquid chromatography; Jmod, J-modulated spin−echo; LED, light-emitting diode; LUMO, lowest unoccupied molecular orbital; MS, mass spectrometry; MTT, 3-(4,5-dimethylthiazol-2-yl)-2,5-diphenyltetrazolium bromide; NIR, near-infrared; NMR, nuclear magnetic resonance; PBS, phosphate-buffered saline; PDT, photodynamic therapy; PS, photosensitizer; ROS, reactive oxygen species; SOSG, Singlet Oxygen Sensor Green; TDDFT, time-dependent density functional theory; TEAA, triethylammonium acetate; TFA, trifluoroacetic acid; tiron, 1,2-dihydroxybenzene-3,5-disulfonic acid disodium salt hydrate; UV−vis, ultraviolet−visible

■ REFERENCES

(1) Stefflova, K.; Chen, J.; Zheng, G. Using Molecular Beacons for Cancer Imaging and Treatment. *Front. Biosci.* **2007**, *12*, 4709−4721.
(2) Stefflova, K.; Chen, J.; Zheng, G. Killer Beacons for Combined Cancer Imaging and Therapy. *Curr. Med. Chem.* **2007**, *14*, 2110−2125.
(3) Lovell, J. F.; Liu, T. W. B.; Chen, J.; Zheng, G. Activatable Photosensitizers for Imaging and Therapy. *Chem. Rev.* **2010**, *110*, 2839−2857.
(4) O'Connor, A. E.; Gallagher, W. M.; Byrne, A. T. Porphyrin and Nonporpyrin Photosensitizers in Oncology: Preclinical and Clinical Advances in Photodynamic Therapy. *Photochem. Photobiol.* **2009**, *85*, 1053−1074.
(5) Allison, R. R.; Sibata, C. H. Oncologic Photodynamic Therapy Photosensitizers: A Clinical Review. *Photodiagn. Photodyn. Ther.* **2010**, *7*, 61−75.
(6) Allison, R. R.; Downie, G. H.; Cuenca, R.; Hu, X.-H.; Childs, C. J. H.; Sibata, C. H. Photosensitizers in Clinical PDT. *Photodiagn. Photodyn. Ther.* **2004**, *1*, 27−42.
(7) Plaetzer, K.; Krammer, B.; Berlanda, J.; Berr, F.; Kiesslich, T. Photophysics and Photochemistry of Photodynamic Therapy: Fundamental Aspects. *Lasers Med. Sci.* **2009**, *24*, 259−268.
(8) Kelleher, D. K.; Thews, O.; Scherz, A.; Salomon, Y.; Vaupel, P. Combined Hyperthermia and Chlorophyll-Based Photodynamic Therapy: Tumour Growth and Metabolic Microenvironment. *Br. J. Cancer* **2003**, *89*, 2333−2339.
(9) Dolmans, D. E. J. G. J.; Fukumura, D.; Jain, R. K. Photodynamic Therapy for Cancer. *Nat. Rev. Cancer* **2003**, *3*, 380−387.
(10) Zhao, J.; Wu, W.; Sun, J.; Guo, S. Triplet Photosensitizers: From Molecular Design to Applications. *Chem. Soc. Rev.* **2013**, *42*, 5323−5351.
(11) Oertel, M.; Schastak, S. I.; Tannapfel, A.; Hermann, R.; Sack, U.; Mössner, J.; Berr, F. Novel Bacteriochlorine for High Tissue-Penetration: Photodynamic Properties in Human Biliary Tract Cancer Cells in Vitro and in a Mouse Tumour Model. *J. Photochem. Photobiol., B* **2003**, *71*, 1−10.
(12) Scherz, A.; Salomon, Y.; Brandis, A.; Scheer, H. Palladium-Substituted Bacteriochlorophyll Derivatives and Use Thereof. U.S. Patent 6,569,846 B1, 2003.
(13) Huang, Z.; Chen, Q.; Luck, D.; Beckers, J.; Wilson, B. C.; Trncic, N.; LaRue, S. M.; Blanc, D.; Hetzel, F. W. Studies of a Vascular-Acting Photosensitizer, Pd-Bacteriopheophorbide (Tookad), in Normal Canine Prostate and Spontaneous Canine Prostate Cancer. *Lasers Surg. Med.* **2005**, *36*, 390−397.
(14) Weersink, R. A.; Forbes, J.; Bisland, S.; Trachtenberg, J.; Elhilali, M.; Brún, P.-H.; Wilson, B. C. Assessment of Cutaneous Photosensitivity of Tookad (WST09) in Preclinical Animal Models and in Patients. *Photochem. Photobiol.* **2005**, *81*, 106−113.
(15) Huang, Z.; Chen, Q.; Trncic, N.; LaRue, S.; Brún, P.-H.; Wilson, B. C.; Shapiro, H.; Hetzel, F. W. Effects of Pd-Bacteriopheophorbide (Tookad)-Mediated Photodynamic Therapy on Canine Prostate Pretreated with Ionizing Radiation. *Radiat. Res.* **2004**, *161*, 723−731.
(16) Koudinova, N. V.; Pinthus, J. H.; Brandis, A.; Brenner, O.; Bendel, P.; Ramon, J.; Eshhar, Z.; Scherz, A.; Salomon, Y. Photodynamic Therapy with Pd-Bacteriopheophorbide (Tookad): Successful in Vivo Treatment of Human Prostatic Small Cell Carcinoma Xenografts. *Int. J. Cancer.* **2003**, *104*, 782−789.
(17) Vakrat-Haglili, Y.; Weiner, L.; Brumfeld, V.; Brandis, A.; Salomon, Y.; McIlroy, B.; Wilson, B. C.; Pawlak, A.; Rozanowska, M.; Sarna, T.; Scherz, A. The Microenvironment Effect on the Generation of Reactive Oxygen Species by Pd-Bacteriopheophorbide. *J. Am. Chem. Soc.* **2005**, *127*, 6487−6497.

(18) Scherz, A.; Salomon, Y.; Mazor, O.; Scheer, H. Water-Soluble Anionic Bacteriochlorophyll Derivatives and Their Uses. U.S. Patent 2006/0142260 A1, 2006.
(19) Brandis, A.; Mazor, O.; Neumark, E.; Rosenbach-Belkin, V.; Salomon, Y.; Scherz, A. Novel Water-Soluble Bacteriochlorophyll Derivatives for Vascular-Targeted Photodynamic Therapy: Synthesis, Solubility, Phototoxicity and the Effect of Serum Proteins. *Photochem. Photobiol.* **2005**, *81*, 983−993.
(20) Berdugo, M.; Bejjani, R. A.; Valamanesh, F.; Savoldelli, M.; Jeanny, J.-C.; Blanc, D.; Ficheux, H.; Scherz, A.; Salomon, Y.; BenEzra, D.; Behar-Cohen, F. Evaluation of the New Photosensitizer Stakel (WST-11) for Photodynamic Choroidal Vessel Occlusion in Rabbit and Rat Eyes. *Invest. Ophthalmol. Visual Sci.* **2008**, *49*, 1633−1644.
(21) Chevalier, S.; Anidjar, M.; Scarlata, E.; Hamel, L.; Scherz, A.; Ficheux, H.; Borenstein, N.; Fiette, L.; Elhilali, M. Preclinical Study of the Novel Vascular Occluding Agent, WST11, for Photodynamic Therapy of the Canine Prostate. *J. Urol.* **2011**, *186*, 302−309.
(22) Goldshaid, L.; Rubinstein, E.; Brandis, A.; Segal, D.; Leshem, N.; Brenner, O.; Kalchenko, V.; Eren, D.; Yecheskel, T.; Salitra, Y.; Salomon, Y.; Scherz, A. Novel Design Principles Enable Specific Targeting of Imaging and Therapeutic Agents to Necrotic Domains in Breast Tumors. *Breast Cancer Res.* **2010**, *12*, 1−18.
(23) Mazor, O.; Brandis, A.; Plaks, V.; Neumark, E.; Rosenbach-Belkin, V.; Salomon, Y.; Scherz, A. WST11, A Novel Water-Soluble Bacteriochlorophyll Derivative; Cellular Uptake, Pharmacokinetics, Biodistribution and Vascular-Targeted Photodynamic Activity Using Melanoma Tumors as a Model. *Photochem. Photobiol.* **2005**, *81*, 342−351.
(24) Ashur, I.; Goldschmidt, R.; Pinkas, I.; Salomon, Y.; Szewczyk, G.; Sarna, T.; Scherz, A. Photocatalytic Generation of Oxygen Radicals by the Water-Soluble Bacteriochlorophyll Derivative, WST11, Noncovalently Bound to Serum Albumin. *J. Phys. Chem. A.* **2009**, *113*, 8027−8037.
(25) Huang, L.; Huang, Y.-Y.; Mroz, P.; Tegos, G. P.; Zhiyentayev, T.; Sharma, S. K.; Lu, Z.; Balasubramanian, T.; Krayer, M.; Ruzié, C.; Yang, E.; Kee, H. L.; Kirmaier, C.; Diers, J. R.; Bocian, D. F.; Holten, D.; Lindsey, J. S.; Hamblin, M. R. Stable Synthetic Cationic Bacteriochlorins as Selective Antimicrobial Photosensitizers. *Antimicrob. Agents Chemother.* **2010**, *54*, 3834−3841.
(26) Mroz, P.; Huang, Y.-Y.; Szokalska, A.; Zhiyentayev, T.; Janjua, S.; Nifli, S.-P.; Sherwood, M. E.; Ruzié, C.; Borbas, K. E.; Fan, D.; Krayer, M.; Balasubramanian, T.; Yang, E.; Kee, H. L.; Kirmaier, C.; Diers, J. R.; Bocian, D. F.; Holten, D.; Lindsey, J. S.; Hamblin, M. R. Stable Synthetic Bacteriochlorins Overcome the Resistance of Melanoma to Photodynamic Therapy. *FASEB J.* **2010**, *24*, 1−11.
(27) Yang, E.; Kirmaier, C.; Krayer, M.; Taniguchi, M.; Kim, H.-J.; Diers, J. R.; Bacian, D. F.; Lindsey, J. R.; Holten, D. Photophysical Properties and Electronic Structure of Stable, Tunable, Synthetic Bacteriochlorins: Extending the Features of Native Photosynthetic Pigments. *J. Phys. Chem. B.* **2011**, *115*, 10801−10816.
(28) Llano, J.; Raber, J.; Eriksson, L. A. Theoretical Study of Phototoxic Reactions of Psoralens. *J. Photochem. Photobiol., A* **2003**, *154*, 235−243.
(29) Guedes, R. C.; Eriksson, L. A. Photophysics, Photochemistry, and Reactivity: Molecular Aspects of Perylenequinone Reactions. *Photochem. Photobiol. Sci.* **2007**, *6*, 1089−1096.
(30) Shen, L.; Ji, H.-F.; Zhang, H.-Y. A TDDFT Study on Triplet Excited-State Properties of Curcumin and Its Implications in Elucidating the Photosensitizing Mechanisms of the Pigment. *Chem. Phys. Lett.* **2005**, *409*, 300−303.
(31) Tian, B.; Eriksson, E. S. E.; Eriksson, L. A. Can Range-Separated and Hybrid DFT Functionals Predict Low-Lying Excitations? A Tookad Case Study. *J. Chem. Theory Comput.* **2010**, *6*, 2086−2094.
(32) Vargas, R.; Galván, M.; Vela, A. Singlet-Triplet Gaps and Spin Potentials. *J. Phys. Chem. A.* **1998**, *102*, 3134−3140.
(33) Alberto, M. E.; Iuga, C.; Quartarolo, A. D.; Russo, N. Bisanthracene Bis(dicarboxylic imide)s as Potential Photosensitizers in Photodynamic Therapy: A Theoretical Investigation. *J. Chem. Inf. Model.* **2013**, *53*, 2334−2340.
(34) Eriksson, E. S. E.; Eriksson, L. A. Predictive Power of Long-Range Corrected Functionals on the Spectroscopic Properties of Tetrapyrrole Derivatives for Photodynamic Therapy. *Phys. Chem. Chem. Phys.* **2011**, *13*, 7207−7217.
(35) Mazzone, G.; Russo, N.; Sicilia, E. Theoretical Investigation of the Absorption Spectra and Singlet-Triplet Energy Gap of Positively-Charged Tetraphenylporphyrins as Potential Photodynamic Therapy Photosensitizers. *Can. J. Chem.* **2013**, *91*, 1−5.
(36) Lamsabhi, A. M.; Corral, I.; Pérez, P.; Tapia, O.; Yáñez, M. Oxygenation of the Phenylhalocarbenes. Are They Spin-Allowed or Spin-Forbidden Reactions? *J. Mol. Model.* **2012**, *18*, 2813−2821.
(37) Kozyrev, A. N.; Zheng, G.; Zhu, C.; Dougherty, T. J.; Smith, K. M.; Pandey, R. K. Syntheses of Stable Bacteriochlorophyll-a Derivatives as Potential Photosensitizers for Photodynamic Therapy. *Tetrahedron Lett.* **1996**, *37*, 6431−6434.
(38) Pandey, R. K.; Constantine, S.; Tsuchida, T.; Zheng, G.; Medforth, C. J.; Aoudia, M.; Kozyrev, A. N.; Rodgers, M. A. J.; Kato, H.; Smith, K. M.; Dougherty, T. J. Syntheses, Photophysical Properties, in Vivo Photosensitizing Efficacy, and Human Serum Albumin Binding Properties of Some Novel Bacteriochlorins. *J. Med. Chem.* **1997**, *40*, 2770−2779.
(39) Roxin, Á.; MacDonald, T. D.; Zheng, G. Synthesis and Characterization of a New Natural Product Analog, 13^2-17^3-Bacteriochlorophyllone *a*. *J. Porphyrins Phthalocyanines* [Online early access]. DOI: 10.1142/S1088424613501058. Published Online: Sept **2013**.
(40) Teuchner, K.; Stiel, H.; Leupold, D.; Scherz, A.; Noy, D.; Simonin, I.; Hartwich, G.; Scheer, H. Fluorescence and Excited State Absorption in Modified Pigments of Bacterial Photosynthesis: A Comparative Study of Metal-Substituted Bacteriochlorophylls a. *J. Lumin.* **1997**, *72*−*74*, 612−614.
(41) Taniguchi, M.; Cramer, D. L.; Bhise, A. D.; Kee, H. L.; Bocian, D. F.; Holten, D.; Lindsey, J. S. Accessing the Near-Infrared Spectral Region with Stable, Synthetic, Wavelength-Tunable Bacteriochlorins. *New J. Chem.* **2008**, *32*, 947−958.
(42) Gettinger, C. L.; Heeger, A. J. The Effect of Intrinsic Rigidity on the Optical Properties of PPV Derivatives. *Mol. Cryst. Liq. Cryst.* **1994**, *256*, 507−512.
(43) Abbyad, P.; Childs, W.; Shi, X.; Boxer, S. G. Dynamic Stokes Shift in Green Fluorescent Protein Varients. *Proc. Natl. Acad. Sci. U.S.A.* **2007**, *104*, 20189−20194.
(44) Henary, M.; Mojzych, M.; Say, M.; Strekowski, L. Functionalization of Benzo[*c*,*d*]indole System for the Synthesis of Visible and Near-Infrared Dyes. *J. Heterocycl. Chem.* **2009**, *46*, 84−87.
(45) Chica, R. A.; Moore, M. M.; Allen, B. D.; Mayo, S. L. Generation of Longer Emission Wavelength Red Fluorescent Proteins Using Computationally Designed Libraries. *Proc. Natl. Acad. Sci. U.S.A.* **2010**, *107*, 20257−20262.
(46) Escobedo, J. O.; Rusin, O.; Lim, S.; Strongin, R. M. NIR Dyes for Bioimaging Applications. *Curr. Opin. Chem. Biol.* **2010**, *14*, 64−70.
(47) Piatkevich, K. D.; Malashkevich, V. N.; Morozova, K. S.; Nemkovich, N. A.; Almo, S. C.; Verkhusha, V. V. Extended Stokes Shift in Fluorescent Proteins: Chromophore-Protein Interactions in a Near-Infrared TagRFP675 Variant. *Sci. Rep.* **2013**, *3*, 1−11.
(48) Cohn, C. A.; Simon, S. R.; Schoonen, M. A. A. Comparison of Fluorescence-Based Techniques for the Quantification of Particle-Induced Hydroxyl Radicals. *Part. Fibre Toxicol.* **2008**, *5*, 2-1−2-9.
(49) Castello, P. R.; Drechsel, D. A.; Day, B. J.; Patel, M. Inhibition of Mitochondrial Hydrogen Peroxide Production by Lipophilic Metalloporphyrins. *J. Pharmacol. Exp. Ther.* **2008**, *324*, 970−976.
(50) Šnyrychová, I.; Ayaydin, F.; Hideg, É. Detecting Hydrogen Peroxide in Leaves in Vivo − A Comparison of Methods. *Physiol. Plant.* **2009**, *135*, 1−18.
(51) Fruk, L.; Niemeyer, C. M. Covalent Hemin-DNA Adducts for Generating a Novel Class of Artificial Heme Enzymes. *Angew. Chem., Int. Ed.* **2005**, *44*, 2603−2606.
(52) Widmer, C. C.; Pereira, C. P.; Gehrig, P.; Vallelian, F.; Schoedon, G.; Buehler, P. W.; Schaer, D. J. Hemoglobin Can Attenuate Hydrogen Peroxide-Induced Oxidative Stress by Acting as

an Antioxidative Peroxidase. *Antioxid. Redox Signaling* **2010**, *12*, 185−198.
(53) Fox, R. B.; Harada, R. N.; Tate, R. M.; Repine, J. E. Prevention of Thiourea-Induced Pulmonary Edema by Hydroxyl-Radical Scavengers. *J. Appl. Physiol.* **1983**, *55*, 1456−1459.
(54) Fox, R. B. Prevention of Granulocyte-Mediated Oxidant Lung Injury in Rats by a Hydroxyl Radical Scavenger, Dimethylthiourea. *J. Clin. Invest.* **1984**, *74*, 1456−1464.
(55) Levine, A.; Tenhaken, R.; Lamb, C. H_2O_2 from the Oxidative Burst Orchestrates the Plant Hypersensitive Disease Resistance Response. *Cell* **1994**, *79*, 583−593.
(56) Greenstock, C. L.; Miller, R. W. The Oxidation of Tiron by Superoxide Anion Kinetics of the Reaction in Aqueous Solution and in Chloroplasts. *Biochim. Biophys. Acta* **1975**, *396*, 11−16.
(57) Miller, R. W.; MacDowall, F. D. H. The Tiron Free Radical as a Sensitive Indicator of Chloroplastic Photoautoxidation. *Biochim. Biophys. Acta* **1975**, *387*, 176−187.
(58) Hideg, É.; Spetea, C.; Vass, I. Superoxide Radicals Are Not the Main Promoters of Acceptor-Side-Induced Photoinhibitory Damage in Spinach Thylakoids. *Photosynth. Res.* **1995**, *46*, 399−407.
(59) Price, M.; Reiners, J. J.; Santiago, A. M.; Kessel, D. Monitoring Singlet Oxygen and Hydroxyl Radical Formation with Fluorescent Probes during Photodynamic Therapy. *Photochem. Photobiol.* **2009**, *85*, 1177−1181.
(60) Bancirova, M. Sodium Azide as a Specific Quencher of Singlet Oxygen During Chemiluminescent Detection by Luminol and Cypridina Luciferin Analogues. *Luminescence* **2011**, *26*, 685−688.
(61) Dąbrowski, J. M.; Arnaut, L. G.; Pereira, M. M.; Monteiro, C. J. P.; Urbańska, K.; Simões, S.; Stochel, G. New Halogenated Water-Soluble Chlorin and Bacteriochlorin as Photostable PDT Sensitizers: Synthesis, Spectroscopy, Photophysics, and in Vitro Photosensitizing Efficacy. *ChemMedChem* **2010**, *5*, 1770−1780.
(62) Bezdetnaya, L.; Zeghari, N.; Belitchenko, I.; Barberi-Heyob, M.; Merlin, J.-L.; Potapenko, A.; Guiliemin, F. Spectroscopic and Biological Testing of Photobleaching of Porphyrins in Solution. *Photochem. Photobiol.* **1996**, *64*, 382−386.
(63) Blum, A.; Grossweiner, L. I. Singlet Oxygen Generation by Hematoporphyrin IX, Uroporphyrin I and Hematoporphyrin Derivative at 546 nm in Phosphate Buffer and in the Presence of Egg Phosphatidylcholine Liposomes. *Photochem. Photobiol.* **1985**, *41*, 27−32.
(64) Ragàs, X.; Cooper, L. P.; White, J. H.; Nonell, S.; Flors, C. Quantification of Photosensitized Singlet Oxygen Production by a Fluorescent Protein. *Chem. Phys. Chem.* **2011**, *12*, 161−165.
(65) Dysart, J. S.; Singh, G.; Patterson, M. S. Calculation of Singlet Oxygen Dose from Photosensitizer Fluorescence and Photobleaching During mTHPC Photodynamic Therapy of MLL Cells. *Photochem. Photobiol.* **2005**, *81*, 196−205.
(66) Martínez, L. J.; Sik, R. H.; Chignell, C. F. Fluoroquinolone Antimicrobials: Singlet Oxygen, Superoxide and Phototoxicity. *Photochem. Photobiol.* **1998**, *67*, 399−403.
(67) Dysart, J. S.; Patterson, M. S. Characterization of Photofrin Photobleaching for Singlet Oxygen Dose Estimation During Photodynamic Therapy of MLL Cells in Vitro. *Phys. Med. Biol.* **2005**, *50*, 2597−2616.
(68) Gollmer, A.; Arnbjerg, J.; Blaikie, F. H.; Pedersen, B. W.; Breitenbach, T.; Dassbjerg, K.; Glasius, M.; Ogilby, P. R. Singlet Oxygen Sensor Green®: Photochemical Behavior in Solution and in Mammalian Cell. *Photochem. Photobiol.* **2011**, *87*, 671−679.
(69) Flors, C.; Fryer, M. J.; Waring, J.; Reeder, B.; Bechtold, U.; Mullineaux, P. M.; Nonell, S.; Wilson, M. T.; Baker, N. R. Imaging the Production of Singlet Oxygen In Vivo Using a New Fluorescent Sensor, Singlet Oxygen Sensor Green®. *J. Exp. Bot.* **2006**, *57*, 1725−1734.
(70) Lin, H.; Shen, Y.; Chen, D.; Lin, L.; Wilson, B. C.; Li, B.; Xie, S. Feasibility Study on Quantitative Measurements of Singlet Oxygen Generation Using Singlet Oxygen Sensor Green. *J. Fluoresc.* **2013**, *23*, 41−47.
(71) Shen, Y.; Lin, H. Y.; Huang, Z. F.; Chen, D. F.; Li, B. H.; Xie, S. S. Indirect Imaging of Singlet Oxygen Generation From a Single Cell. *Laser Phys. Lett.* **2011**, *8*, 232−238.
(72) Nakamura, K.; Ishiyama, K.; Ikai, H.; Kanno, T.; Sasaki, K.; Niwano, Y.; Kohno, M. Reevaluation of Analytical Methods for Photogenerated Singlet Oxygen. *J. Clin. Biochem. Nutr.* **2011**, *49*, 87−95.
(73) Monteiro, C. J. P.; Pina, J.; Pereira, M. M.; Arnaut, L. G. On the Singlet States of Porphyrins, Chlorins and Bacteriochlorins and Their Ability to Harvest Red/Infrared Light. *Photochem. Photobiol. Sci.* **2012**, *11*, 1233−1238.
(74) Ding, H.; Yu, H.; Dong, Y.; Tian, R.; Huang, G.; Boothman, D. A.; Sumer, B. D.; Gao, J. Photoactivation Switch from Type II to Type I Reactions by Electron-Rich Micelles for Improved Photodynamic Therapy of Cancer Cells under Hypoxia. *J. Controlled Release* **2011**, *156*, 276−280.
(75) Joshi, P.; Ethirajan, M.; Goswami, L. N.; Srivatsan, A.; Missert, J. R.; Pandey, R. K. Synthesis, Spectroscopic and in-Vitro Photosensitizing Efficacy of Ketobacteriochlorins Derived from Ring-B and Ring-D Reduced Chlorins via Pinacol-Pinacolone Rearrangement. *J. Org. Chem.* **2011**, *76*, 8629−8640.
(76) Silva, E. F. F.; Serpa, C.; Dąbrowski, J. M.; Monteiro, C. J. P.; Formosinho, S. J.; Stochel, G.; Urbanska, K.; Simões, S.; Pereira, M. M.; Arnaut, L. G. Mechanisms of Singlet-Oxygen and Superoxide-Ion Generation by Porphyrins and Bacteriochlorins and Their Implications in Photodynamic Therapy. *Chem.—Eur. J.* **2010**, *16*, 9273−9286.
(77) Georgakoudi, I.; Foster, T. H. Singlet Oxygen- Versus Nonsinglet Oxygen-Mediated Mechanisms of Sensitizer Photobleaching and Their Effects on Photodynamic Therapy. *Photochem. Photobiol.* **1998**, *67*, 612−625.
(78) Bonnett, R.; Djelal, B. D.; Hamilton, P. A.; Mertinez, G.; Wierrani, F. Photobleaching of 5,10,15,20-Tetrakis(m-hydroxyphenyl)porphyrin (m-THPP) and the Corresponding Chlorin (m-THPC) and Bacteriochlorin (m-THPBC). A Comparative Study. *J. Photochem. Photobiol., B.* **1999**, *53*, 136−143.
(79) Bonnett, R.; Martínez, G. Photobleaching of Sensitizers Using in Photodynamic Therapy. *Tetrahedron* **2001**, *57*, 9513−9547.
(80) Dysart, J. S.; Patterson, M. S.; Farrell, T. J.; Singh, G. Relationship Between mTHPC Fluorescence Photobleaching and Cell Viability During in Vitro Photodynamic Treatment of DP16 Cells. *Photochem. Photobiol.* **2002**, *75*, 289−295.
(81) Jarvi, M. T.; Patterson, M. S.; Wilson, B. C. Insights into Photodynamic Therapy Dosimetry: Simultaneous Singlet Oxygen Luminescence and Photosensitizer Photobleaching Measurements. *Biophys. J.* **2012**, *102*, 661−671.